BATF2 inhibits immunopathological Th17 responses by suppressing *Il23a* expression during *Trypanosoma cruzi* infection

Shoko Kitada,[1,2,6]* Hisako Kayama,[1,2,6]* Daisuke Okuzaki,[3] Ritsuko Koga,[7] Masao Kobayashi,[1] Yasunobu Arima,[8] Atsushi Kumanogoh,[4] Masaaki Murakami,[8] Masahito Ikawa,[5] and Kiyoshi Takeda[1,2,6]

[1]Department of Microbiology and Immunology, Graduate School of Medicine, [2]WPI Immunology Frontier Research Center, [3]DNA-Chip Developmental Center for Infectious Diseases, Research Institute for Microbial Diseases, [4]Department of Respiratory Medicine, Allergy and Rheumatic Diseases, Graduate School of Medicine, and [5]Department of Experimental Genome Research, Research Institute for Microbial Diseases, Osaka University, Suita, Osaka 565-0871, Japan
[6]Core Research for Evolutional Science and Technology, Japan Agency for Medical Research and Development, Tokyo 100-0004, Japan
[7]Department of Molecular Genetics, Medical Institute of Bioregulation, Kyushu University, Fukuoka 812-8582, Japan
[8]Division of Molecular Neuroimmunology, Institute for Genetic Medicine, Graduate School of Medicine, Hokkaido University, Sapporo 060-8638, Japan

Inappropriate IL-17 responses are implicated in chronic tissue inflammation. IL-23 contributes to *Trypanosoma cruzi*–specific IL-17 production, but the molecular mechanisms underlying regulation of the IL-23–IL-17 axis during *T. cruzi* infection are poorly understood. Here, we demonstrate a novel function of BATF2 as a negative regulator of *Il23a* in innate immune cells. IL-17, but not IFN-γ, was more highly produced by $CD4^+$ T cells from spleens and livers of *T. cruzi*–infected $Batf2^{-/-}$ mice than by those of wild-type mice. In this context, $Batf2^{-/-}$ mice showed severe multiorgan pathology despite reduced parasite burden. *T. cruzi*–induced IL-23 production was increased in $Batf2^{-/-}$ innate immune cells. The *T. cruzi*–induced enhanced Th17 response was abrogated in $Batf2^{-/-}Il23a^{-/-}$ mice. The interaction of BATF2 with c-JUN prevented c-JUN–ATF-2 complex formation, inhibiting *Il23a* expression. These results demonstrate that IFN-γ–inducible BATF2 in innate immune cells controls Th17-mediated immunopathology by suppressing IL-23 production during *T. cruzi* infection.

INTRODUCTION

Chagas disease, characterized by chronic cardiomyopathy, is caused by infection with the intracellular protozoan parasite *Trypanosoma cruzi* (Bonney et al., 2015). The TLR-MyD88/TRIF adaptor molecule pathways initiate both innate and adaptive immune responses, and thus contribute to the resistance of the host to intracellular protozoan parasites such as *T. cruzi* (Gazzinelli and Denkers, 2006; Kayama and Takeda, 2010; Kawai and Akira, 2011; Rodrigues et al., 2012). Recently, several studies have demonstrated the mechanisms underlying the TLR-independent host defense against *T. cruzi* infection, such as TLR-independent T-helper 1 (Th1) responses (Kayama et al., 2009).

Th17 cells, which produce IL-17A, IL-17F, IL-22, and GM-CSF, play essential roles in the immune response to infection (Miyazaki et al., 2010; McGeachy and McSorley, 2012; Bermejo et al., 2013). Th17 cell differentiation is induced by IL-6 and TGF-β, and IL-23 mediates the enhanced production of Th17 cell–related cytokines (Gaffen et al., 2014). IL-17A–producing $CD4^+$ T cells are greatly increased in mice infected with *T. cruzi* (da Matta Guedes et al., 2010), and a lack of IL-17A is linked to the aggravation of the parasite burden and the failure of various organs after *T. cruzi* infection (da Matta Guedes et al., 2010; Miyazaki et al., 2010). These findings indicate that adequate IL-17 responses are required for host protection, but that enhanced IL-17 production can cause tissue immunopathology during infection with intracellular protozoan parasites. Several studies have demonstrated that the Th17 response, particularly induction of Th17 cell development, is tightly regulated by several mechanisms during the course of parasite infection. For example, the IL-27/WSX-1 signaling pathway plays an important role in the negative regulation of IL-17 production by $CD4^+$ T cells during *T. cruzi* and *Toxoplasma gondii* infection (Stumhofer et al., 2006; Yoshimura et al., 2006), and the T cell-intrinsic transcription factor T-bet, encoded by *Tbx21*, contributes to the inhibition of *T. cruzi*–specific Th17 cell differentiation (Guo et al., 2009). IL-12p35 also down-regulates Th17 responses to *T. cruzi* (Cobb and Smeltz, 2012). However, it remains unclear how Th17 cell responses are controlled after induction.

IL-23, a heterodimer of the IL-23p19 and IL-12p40 subunits, is essential for the generation of pathogenic Th17 cells (McGeachy et al., 2009; Gaffen et al., 2014). In experimental autoimmune myocarditis (EAM), IL-23 functions as a key effector molecule by promoting the production of

*S. Kitada and H. Kayama contributed equally to this paper.

Correspondence to Kiyoshi Takeda: ktakeda@ongene.med.osaka-u.ac.jp

Abbreviations used: AST, aspartate aminotransferase; BMMφ, BM-derived Mφ; ChIP, chromatin immunoprecipitation; CK, creatinine kinase; CRE, creatinine; Mφ, macrophage; PEC, peritoneal Mφ; qPCR, quantitative PCR.

The Rockefeller University Press $30.00
J. Exp. Med. 2017 Vol. 214 No. 5 1313–1331
https://doi.org/10.1084/jem.20161076

IL-17 by lymphocytes (Rangachari et al., 2006). IL-23 is also implicated in the development of colitis by stimulating the accumulation of Th17 cells (Ahern et al., 2010). In contrast, another study has shown that induction of histone modification by IFN-γ was linked to the suppression of *Il23a* expression, which encodes IL-23p19, in intestinal CD11b$^+$ Mφs, thus preventing colitis (Sheikh et al., 2010). The IFN-γ released by CD8$^+$ T cells also suppresses the development of EAM through inhibition of IL-17 production (Rangachari et al., 2006). These findings indicate that the IL-23–Th17 axis is tightly regulated by IFN-γ in a variety of contexts. *T. cruzi* infection induces IL-23 production by host immune cells, and antigen-specific Th17 responses are then promoted (Cobb et al., 2010; Erdmann et al., 2013). However, whether the IL-23–Th17 axis is controlled by IFN-γ–dependent mechanisms during *T. cruzi* infection remains unclear.

Transcription factor BATF2 was initially identified as an AP-1 inhibitor (Su et al., 2008). In cancer cells, BATF2 suppresses the expression of AP-1–dependent genes through its interaction with c-JUN (Su et al., 2008). In contrast, BATF2 functions as a transcriptional activator in BM-derived macrophages (Mφs [BMMφs]) by interacting with IRF1 in response to IFN-γ and the TLR4 ligand LPS (Roy et al., 2015). BATF2 also compensates CD103$^+$ DC development in *Batf3*$^{-/-}$ mice (Tussiwand et al., 2012). We previously demonstrated that BATF2 is normally induced in *Myd88*$^{-/-}$*Trif*$^{-/-}$ BM-derived DCs (BMDCs) during *T. cruzi* infection (Kayama et al., 2009). However, the roles of IFN-γ–inducible BATF2 in *T. cruzi*–infected innate immune cells are poorly understood.

In this study, we demonstrate the mechanism by which BATF2 regulates *T. cruzi*–specific IL-17 production by CD4$^+$ T cells. IFN-γ–inducible BATF2 inhibits *Il23a* expression in DCs and Mφs during *T. cruzi* infection by disrupting the formation of the c-JUN–ATF-2 complex by directly binding to c-JUN, thus preventing Th17-mediated tissue damage during *T. cruzi* infection. Therefore, BATF2-mediated modulation of the IL-23–Th17 axis is involved in host resistance to *T. cruzi* infection.

RESULTS

IFN-γ–induced expression of BATF2

We previously demonstrated the TLR-independent expression of *4933430F08Rik*, encoding BATF2, in *T. cruzi*–infected BMDCs (Kayama et al., 2009). To assess the physiological role of BATF2 during *T. cruzi* infection, we generated *Batf2*$^{-/-}$ mice with gene targeting (Fig. S1, A and B). Stimulation with LPS plus IFN-γ robustly induced BATF2 mRNA in wild-type BMMφs, but not *Batf2*$^{-/-}$ BMMφs (Fig. S1 C). In wild-type BMMφs, IFN-γ, but not LPS, induced high levels of *Batf2* expression (Fig. S1 D). The expression of the mRNAs of other BATF family members, such as BATF and BATF3, was not induced by IFN-γ in BMMφs (Fig. S1 E). Moreover, BATF2 deficiency did not lead to the compensatory up-regulation of *Batf* and *Batf3* expression, as previously described (Roy et al., 2015; Fig. S1 E). A subset of TLR-independent genes shown to be expressed in *Myd88*$^{-/-}$*Trif*$^{-/-}$ BMDCs during *T. cruzi* infection (Kayama et al., 2009) was normally induced in *Batf2*$^{-/-}$ BMMφs stimulated with IFN-γ (Fig. S1 F). These results indicate that BATF2 is not involved in the expression of a subset of IFN-γ–inducible genes.

To determine whether BATF2 is responsible for immune cell development, we analyzed the composition of both lymphocytes and innate myeloid cells in the spleens of wild-type and *Batf2*$^{-/-}$ mice (Fig. S1 G). The frequencies and total cell numbers of the CD11c$^+$ CD103$^+$, CD11b$^+$ Ly-6C$^+$, CD11b$^+$ Ly-6G$^+$, CD3$^+$ CD4$^+$, CD3$^+$ CD8$^+$, and B220$^+$ CD19$^+$ cell populations were not altered in the *Batf2*$^{-/-}$ mice, demonstrating that the development of neither innate nor adaptive immune cells was affected in *Batf2*$^{-/-}$ mice.

Increased production of IL-17, but not IFN-γ, by CD4$^+$ T cells in *T. cruzi*–infected *Batf2*$^{-/-}$ mice

The TLR-independent production of IFN-γ by innate immune cells is implicated in driving Th1 responses during *T. cruzi* infection (Kayama et al., 2009). Because BATF2 was shown to be induced by a TLR-independent IFN-γ–dependent mechanism, we analyzed whether BATF2 is responsible for the induction of Th1 responses during *T. cruzi* infection. Wild-type and *Batf2*$^{-/-}$ mice were intraperitoneally infected with *T. cruzi* trypomastigotes. CD4$^+$ T cells were isolated from their spleens 0, 15, 20, and 30 d after infection, whereas liver CD4$^+$ T cells were isolated 15, 20, and 30 d after infection because there were fewer of these cells in the uninfected mice. The isolated CD4$^+$ T cells were stimulated with anti-CD3 antibody (Fig. 1 A). The spleen CD4$^+$ T cells of *T. cruzi*–infected wild-type mice showed considerably higher production of IFN-γ at 15, 20, and 30 d of infection than the uninfected mice, indicating induction of an intensive Th1 response. IFN-γ production by the spleen CD4$^+$ T cells of *T. cruzi*–infected *Batf2*$^{-/-}$ mice was similar to that of wild-type mice. Furthermore, no difference in IFN-γ production was observed in liver CD4$^+$ T cells of the wild-type and *Batf2*$^{-/-}$ mice after *T. cruzi* infection (Fig. 1 B). We next analyzed antigen-specific Th1 responses after infection by stimulating CD4$^+$ T cells with freeze-thawed *T. cruzi* in the presence of antigen-presenting cells (Fig. 1, C and D). IFN-γ production by the *Batf2*$^{-/-}$ CD4$^+$ T cells from the spleen and liver at any time point of infection was similar to that by wild-type CD4$^+$ T cells, indicating that the Th1 responses during *T. cruzi* infection were not impaired in *Batf2*$^{-/-}$ mice.

Recent studies have shown that IL-17 is responsible for host resistance to *T. cruzi* infection (da Matta Guedes et al., 2010; Miyazaki et al., 2010; Bermejo et al., 2013). Therefore, we examined IL-17 production by CD4$^+$ T cells in the spleens and livers of *T. cruzi*–infected mice. More IL-17 was produced by CD4$^+$ T cells from the spleens of *T. cruzi*–infected wild-type mice stimulated with anti-CD3 antibody than from uninfected mice (Fig. 1 E). These findings indicate that *T. cruzi* infection causes the induction of Th17 immune responses. At 20- and 30-d time points of infection, IL-17 production by

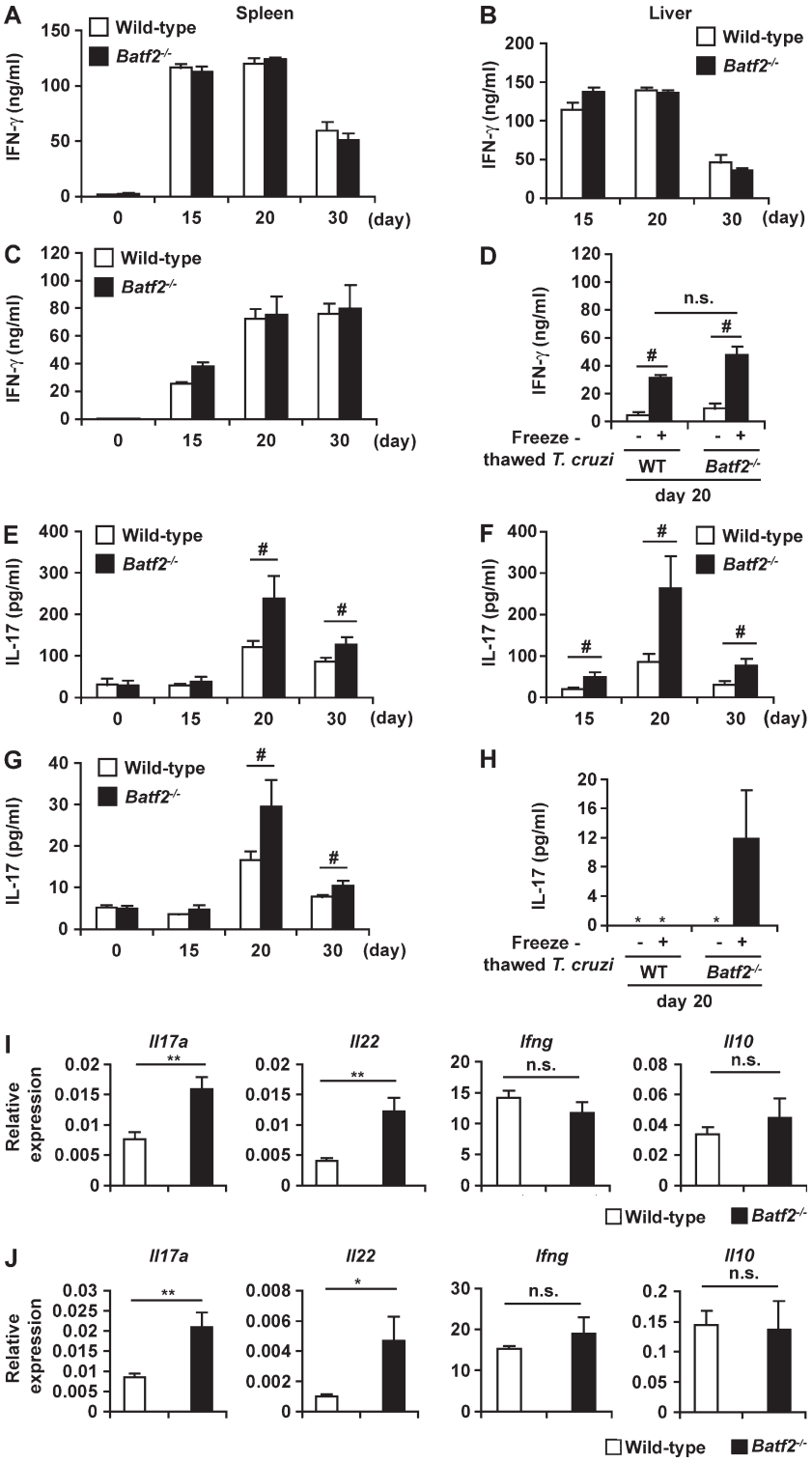

Figure 1. **Increased production of IL-17 in CD4$^+$ T cells in *T. cruzi*–infected *Batf2*$^{-/-}$ mice.** (A–H) CD4$^+$ T cells were isolated from the spleens (left) and livers (right) of wild-type (WT) and *Batf2*$^{-/-}$ mice at 0 d (n = 5 per group), 15 d (n = 6 per group), 20 d (n = 8 per group), and 30 d (n = 5 per group) of *T. cruzi* infection. Isolated CD4$^+$ T cells were stimulated with anti-CD3 antibody (A, B, E, and F) or heat-killed *T. cruzi* (C, D, G, and H) and analyzed for IFN-γ and IL-17 with ELISA. Graphs show mean values ± SEM. *, not detected; #, $P < 0.05$; n.s., not significant. (I and J) Expression of *Il17a*, *Il22*, *Il10*, and *Ifng* in CD4$^+$ T cells was isolated from spleens (I) and livers (J) of wild-type (n = 5) and *Batf2*$^{-/-}$ (n = 4) mice after *T. cruzi* infection for 20 d (mean values ± SEM). *, $P < 0.05$; **, $P < 0.01$; n.s., not significant.

CD4$^+$ T cells stimulated with anti-CD3 antibody was considerably higher in the spleens of *T. cruzi*–infected *Batf2*$^{-/-}$ mice than in those of wild-type mice (Fig. 1 E). In the liver, IL-17 production by anti-CD3 antibody–stimulated *Batf2*$^{-/-}$ CD4$^+$ T cells was greatly increased at 15, 20, and 30 d of infection compared with wild-type cells (Fig. 1 F). Furthermore, antigen-specific IL-17 production was markedly higher after *T. cruzi* infection in *Batf2*$^{-/-}$ spleen and liver CD4$^+$ T cells than in the corresponding wild-type cells (Fig. 1, G and H). Intracellular staining analysis also showed that production

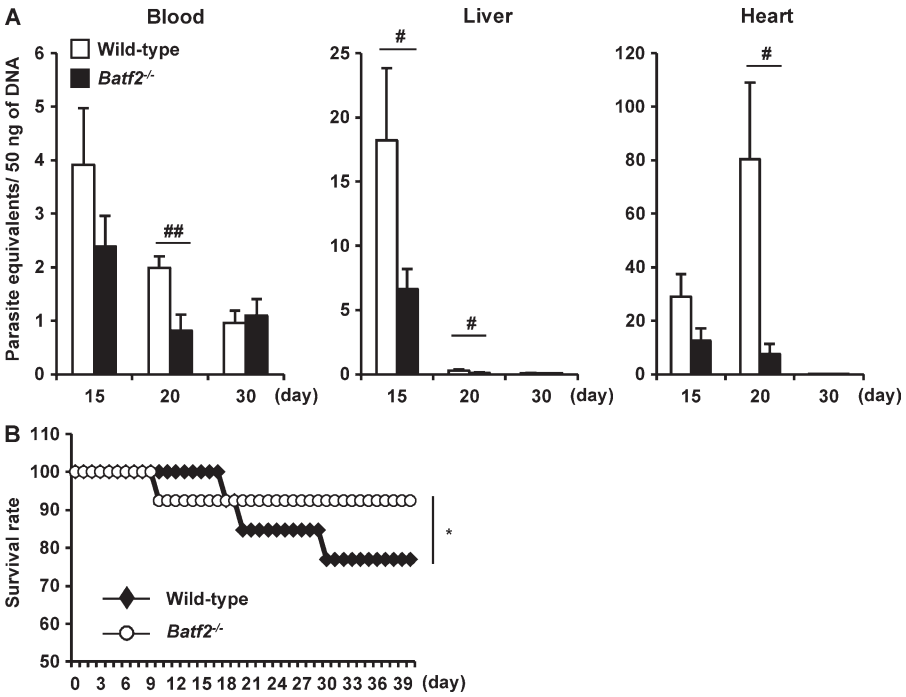

Figure 2. **Lower levels of parasitemia in *T. cruzi*–infected *Batf2*$^{-/-}$ mice.** (A) Parasite equivalents in the livers, hearts, and blood of wild-type and *Batf2*$^{-/-}$ mice 15, 20, and 30 d after infection ($n \geq 5$). $^{\#}$, $P < 0.05$; $^{\#\#}$, $P < 0.009$. Data are mean values ± SEM. (B) Mortality of wild-type and *Batf2*$^{-/-}$ mice after *T. cruzi* infection. Line graphs represent data pooled from three independent experiments ($n = 13$). *, $P = 0.036$.

of IL-17, but not IFN-γ and IL-10, was increased in CD4$^+$ T cells from the spleens and livers of *T. cruzi*–infected *Batf2*$^{-/-}$ mice compared with those from wild-type mice, as indicated by increased mean fluorescence intensity of IL-17 (Fig. S2, A, B, D, and E). In addition, a higher frequency of IFN-γ$^+$ IL-17$^+$ CD4$^+$ T cells was observed in the spleens, but not livers, of *Batf2*$^{-/-}$ mice (Fig. S2, C and F). Expression of Th17-related genes, such as *Il17* and *Il22*, was markedly higher in CD4$^+$ T cells from the spleens and livers of *T. cruzi*–infected *Batf2*$^{-/-}$ mice than in the corresponding cells from wild-type mice (Fig. 1, I and J), whereas expression of *Ifng* and *Il10* in *Batf2*$^{-/-}$ CD4$^+$ T cells was similar to that in wild-type cells. These findings indicate that BATF2 modulates Th17 responses during *T. cruzi* infection.

Increased multiorgan pathology in *T. cruzi*–infected *Batf2*$^{-/-}$ mice

We next assessed parasitemia levels in the blood, livers, and hearts of wild-type and *Batf2*$^{-/-}$ mice after infection, using quantitative PCR (qPCR) assay to measure the amounts of *T. cruzi* DNA (Fig. 2 A). In the blood and livers of *T. cruzi*–infected wild-type mice, the parasite number increased as early as 15 d and then gradually decreased. In *T. cruzi*–infected *Batf2*$^{-/-}$ mice, the parasite number was reduced, particularly at 20 d of infection, compared with wild-type mice. In the hearts of *T. cruzi*–infected wild-type mice, the parasite number increased slowly and reached peak levels at 20 d. The parasite number in the hearts was dramatically reduced in *Batf2*$^{-/-}$ mice. In accordance with the reduced parasite burden, *Batf2*$^{-/-}$ mice showed higher survival rates compared with wild-type mice after *T. cruzi* infection (Fig. 2 B). We also analyzed pathological changes (Fig. 3, A and B) in the livers and hearts of *T. cruzi*–infected wild-type and *Batf2*$^{-/-}$ mice. There was greater hepatic inflammation and myocarditis in *Batf2*$^{-/-}$ mice after *T. cruzi* infection than in wild-type mice. We then measured the concentrations of markers for tissue damage: aspartate aminotransferase (AST) in the plasma, which is indicative of liver damage; creatinine kinase (CK) in the plasma, indicative of heart failure; and creatinine (CRE) in the serum, indicative of renal failure (Miyazaki et al., 2010; Fig. 3 C). AST, CK, and CRE were markedly higher in *T. cruzi*–infected *Batf2*$^{-/-}$ mice than in wild-type mice. The expression of *Mpo*, which encodes myeloperoxidase, a tissue-damaging factor produced by neutrophils, was elevated in the spleens, livers, and mesenteric LNs (MLNs) of *T. cruzi*–infected *Batf2*$^{-/-}$ mice (Fig. 3 D). We also analyzed the expression of Th17-related genes, such as *Il17a*, *Il22*, and *Csf2*, in the spleens, livers, and MLNs of wild-type and *Batf2*$^{-/-}$ mice after *T. cruzi* infection (Fig. 3 E). Expression of these Th17-related genes was extremely enhanced in all tissues of *Batf2*$^{-/-}$ mice compared with those of wild-type mice. Thus, enhanced Th17 responses correlated with heightened immune activation and tissue damage, despite reduced parasite numbers and mortality, in *T. cruzi*–infected *Batf2*$^{-/-}$ mice.

Increased LPS-induced IL-23 production by *Batf2*$^{-/-}$ innate immune cells

To determine the mechanisms by which BATF2 modulates Th17 responses during *T. cruzi* infection, we first examined whether T cell-intrinsic BATF2 is involved in either the generation of Th17 cells or the production of IL-17 by CD4$^+$ T cells. Naive CD4$^+$ T cells isolated from the spleens of wild-

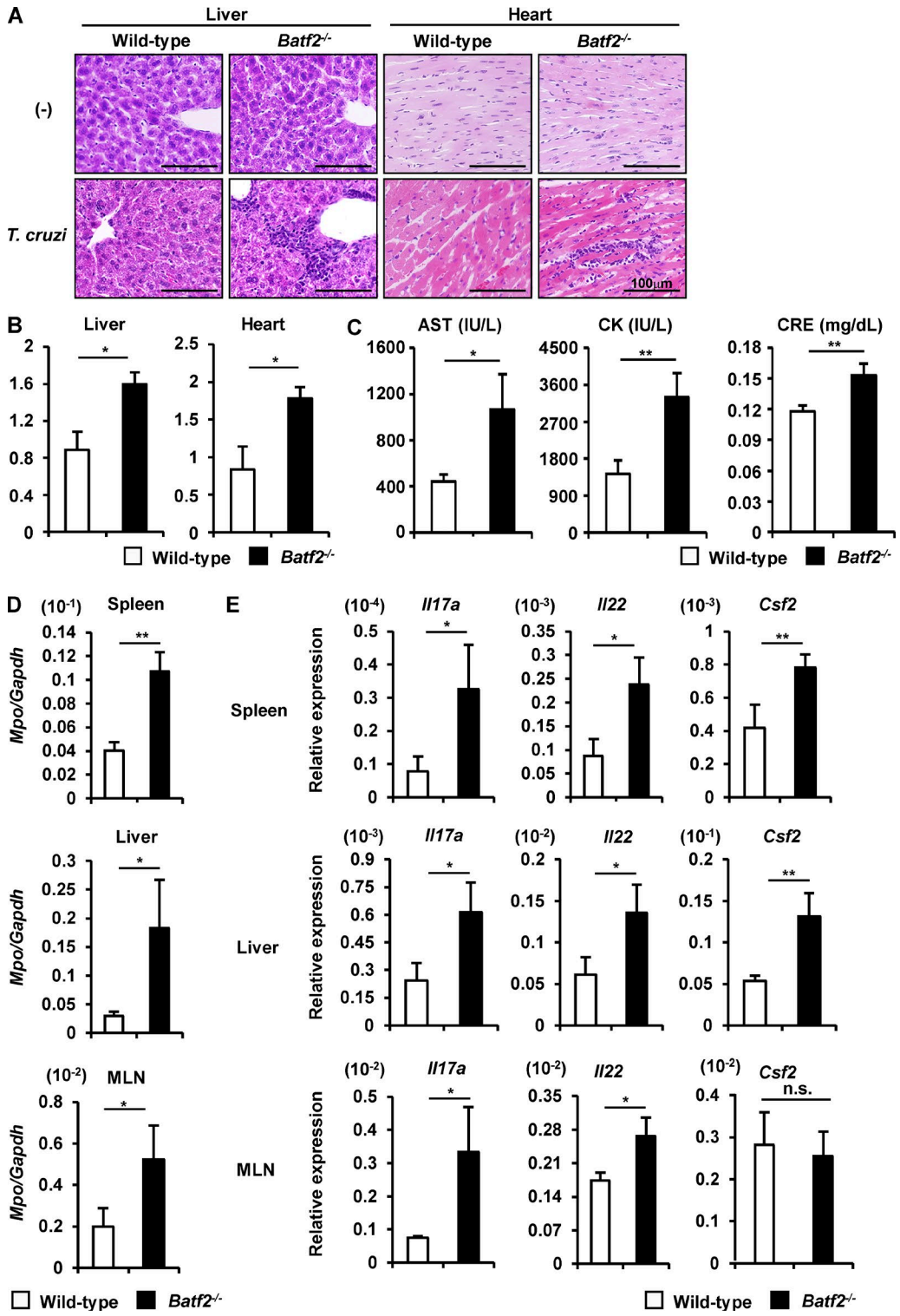

Figure 3. **Severe multiorgan pathology in *T. cruzi*–infected *Batf2*$^{-/-}$ mice.** (A and B) Representative histopathology (A) and histopathological score (B) of wild-type (n = 8) and *Batf2*$^{-/-}$ (n = 9) mice 49 d after infection. Bars, 100 µm. Graphs show mean values ± SD. *, P < 0.01. (C) Concentrations of AST and CK in the plasma and CRE in tge sera of *T. cruzi*–infected wild-type ($n \geq 14$) and *Batf2*$^{-/-}$ ($n \geq 19$) mice. *, P < 0.05; **, P < 0.01. Graphs are mean values ± SEM. (D) *Mpo* expression in tissues of wild-type and *Batf2*$^{-/-}$ mice after *T. cruzi* infection (n = 3 per group). *, P < 0.05; **, P < 0.02. Data are mean values ± SEM. (E) Expression of Th17-related genes (n = 4 per group). *, P < 0.05; **, P < 0.02; n.s., not significant. All graphs show mean values ± SEM.

type and *Batf2*$^{-/-}$ mice were cultured under Th0, Th1, or Th17 conditions for 4 d and then analyzed for IFN-γ and IL-17 production with intracellular staining and ELISA. The frequency of IL-17–producing cells among *Batf2*$^{-/-}$ CD4^{+} T cells cultured under Th17 conditions was similar to that in wild-type cells (Fig. S3 A). Moreover, IFN-γ–producing *Batf2*$^{-/-}$ CD4^{+} T cells maintained under Th1 conditions were induced to levels similar to those in wild-type cells. There was no significant difference in the secretion of IL-17 or IFN-γ by wild-type and *Batf2*$^{-/-}$ CD4^{+} T cells stimulated with anti-CD3 antibody (Fig. S3 B), indicating that T cell–intrinsic BATF2 does not affect the differentiation of Th1 and Th17 cells or their cytokine production.

Accumulating evidence has shown that the Th17 responses are tightly controlled by the innate immune cells (Gaffen et al., 2014). Therefore, to determine the functions of BATF2 in innate immune responses, we comprehensively analyzed the overall gene expression patterns in wild-type and *Batf2*$^{-/-}$ BMMφs. RNA-seq analysis showed that 98 genes are up-regulated in *Batf2*$^{-/-}$ BMMφs stimulated with LPS and IFN-γ relative to their expression in wild-type cells (Table S1). Among these genes, we focused on *Il23a*, which encodes IL-23p19, because IL-23 promotes the expression of *Il17a* in Th17 cells (Gaffen et al., 2014). To confirm the results of the RNA-seq analysis, we examined LPS-induced expression of *Il23a*, *Il6*, *Tnf*, and *Il12b* in IFN-γ–pretreated innate immune cells prepared from wild-type and *Batf2*$^{-/-}$ mice, using real-time RT-PCR. The expression of *Il23a*, but not *Il6*, *Tnf*, or *Il12b*, was dramatically higher in *Batf2*$^{-/-}$ Mφs, such as peritoneal Mφs (PECs) and BMMφs, than in wild-type cells (Fig. 4, A and B). *Batf2*$^{-/-}$ BMDCs also showed higher expression of *Il23a* than wild-type BMDCs (Fig. 4 C). Because an increase in *Il23a* expression was observed in *Batf2*$^{-/-}$ innate immune cells, we next analyzed the LPS-induced production of proinflammatory cytokines in wild-type and *Batf2*$^{-/-}$ innate immune cells pretreated with IFN-γ. Consistent with the mRNA expression patterns, the production of IL-23 by IFN-γ–pretreated *Batf2*$^{-/-}$ PECs, BMMφs, and BMDCs was markedly higher than that by wild-type cells, whereas IL-6, TNF, and IL-12p40 were normally produced by the *Batf2*$^{-/-}$ cells (Fig. 4, D–F). We also analyzed LPS-induced cytokine production by IFN-γ–untreated innate immune cells. IFN-γ–untreated *Batf2*$^{-/-}$ and wild-type PECs, BMMφs, and BMDCs produced similar amounts of IL-23 as well as IL-6, TNF, and IL-12p40 in response to LPS (Fig. S4, A–C). LPS-induced *Il23a* expression is negatively regulated by an IFN-γ–dependent mechanism in Mφs (Sheikh et al., 2010). Therefore, we evaluated the LPS-induced production of IL-23 at the mRNA and protein levels in wild-type and *Batf2*$^{-/-}$ BMMφs pretreated with or without IFN-γ (Fig. 4 G and Fig. S4 D). LPS stimulation robustly induced IL-23 expression in the wild-type BMMφs, whereas IFN-γ pretreatment dramatically reduced this LPS-induced IL-23 expression. In the *Batf2*$^{-/-}$ BMMφs not pretreated with IFN-γ, the expression of IL-23 in response to LPS was similar to that in wild-type BMMφs, but the IFN-γ–induced reduction in IL-23 expression was lower in *Batf2*$^{-/-}$ cells stimulated with LPS than in stimulated wild-type cells. To investigate whether the newly synthesized proteins induced by IFN-γ are involved in the inhibition of LPS-induced *Il23a* expression in innate immune cells, BMMφs were pretreated with IFN-γ in the presence or absence of cycloheximide (CHX), an inhibitor of protein synthesis, and then stimulated with LPS (Fig. S4 E). Compared with control cells, LPS-induced *Il23a* expression was greatly increased in CHX-treated cells. Collectively, these findings suggest that IFN-γ–induced BATF2 contributes to the suppression of the LPS-dependent expression of *Il23a*, but not *Il6*, *Tnf*, or *Il12b*, in innate immune cells.

BATF2-mediated suppression of IL-23 production by innate immune cells during *T. cruzi* infection

In the next experiment, we analyzed the effect of BATF2 on *T. cruzi*–induced IL-23 production. *Batf2* expression was highest 6 h after *T. cruzi* infection, and this was maintained in both BMMφs and BMDCs even after 12 h of infection (Fig. 5 A). BMMφs and BMDCs prepared from wild-type and *Batf2*$^{-/-}$ mice were pretreated with or without IFN-γ for 4 h, exhaustively washed, and then infected with *T. cruzi*. At 24 h after infection, the culture supernatants were analyzed for IL-23, IL-6, IL-12p40, and IL-12p70 with ELISA (Fig. 5, B and C). Even in the absence of IFN-γ pretreatment, *Batf2*$^{-/-}$ cells showed higher levels of *T. cruzi*–mediated IL-23 production than wild-type cells. The enhanced *T. cruzi*–dependent response was specific to IL-23, because IL-6, IL-12p40, and IL-12p70 production and expression of I-A^{b}, CD80, and CD86 were normally increased in *T. cruzi*–infected *Batf2*$^{-/-}$ BMDCs (Fig. 5, C and D). IFN-γ pretreatment caused reduced production of IL-23, but not IL-6, IL-12p40, and IL-12p70, in *T. cruzi*–infected wild-type cells (Fig. 5, B and C). However, only a partial reduction in IL-23 production was observed in *Batf2*$^{-/-}$ cells. To investigate the involvement of BATF2 in the replication of *T. cruzi* within innate immune cells, BMMφs prepared from wild-type and *Batf2*$^{-/-}$ mice were pretreated with or without IFN-γ and infected with *T. cruzi*. At 6 h after infection, cells were thoroughly washed and changed to fresh media. At 72 h of culture, intracellular *T. cruzi* numbers in the wild-type BMMφs were decreased in an IFN-γ dose–dependent manner (Fig. 5 E). The numbers of intracellular parasites in *Batf2*$^{-/-}$ BMMφs were similarly reduced as IFN-γ concentration increased. Moreover, the numbers of trypomastigotes desorbed into the culture supernatant of the *Batf2*$^{-/-}$ BMMφs were similar to those of wild-type cells at 3, 4, 5, and 7 d after *T. cruzi* infection (Fig. 5 F). These findings indicate that BATF2 is required for the down-regulation of *T. cruzi*–induced IL-23 production in innate immune cells, but not for the killing of *T. cruzi*.

We then analyzed whether IFN-γ is responsible for the suppression of IL-23 production by *T. cruzi*–infected innate immune cells. BMMφs and BMDCs prepared from wild-type and *Ifng*$^{-/-}$ mice were infected with *T. cruzi* and cultured for

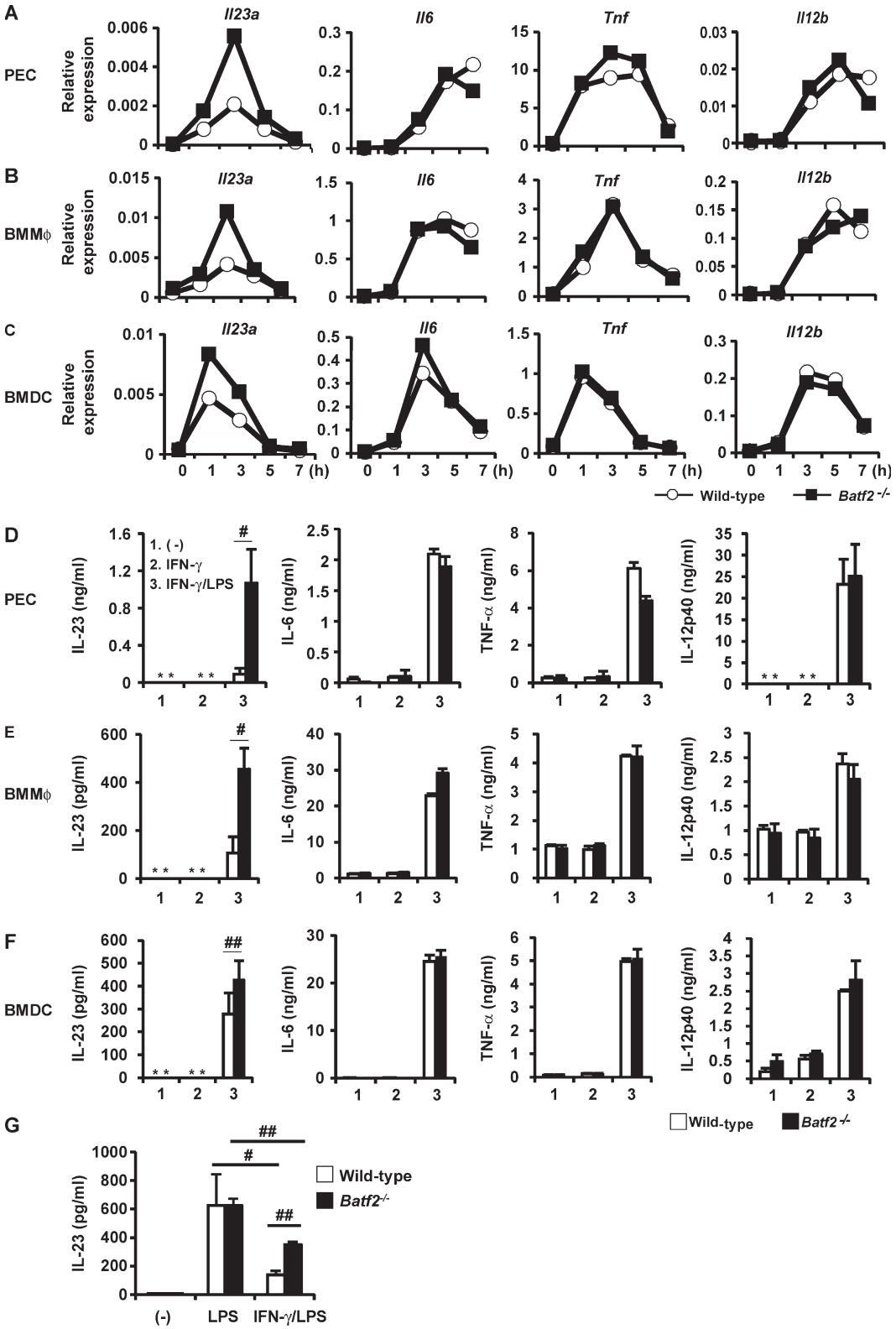

Figure 4. **Increased IL-23 production by *Batf2*$^{-/-}$ innate immune cells stimulated with LPS after IFN-γ treatment.** (A–C) Expression of *Il23a*, *Il6*, *Tnf*, and *Il12b* in wild-type and *Batf2*$^{-/-}$ PECs (A), BMMφs (B), and BMDCs (C). All data are representative of at least two independent experiments. (D–F) Production of IL-23, IL-6, IL-12p40, and TNF by wild-type and *Batf2*$^{-/-}$ PECs (D), BMMφs (E), and BMDCs (F). Results are mean ± SEM from four independent experiments. *, not detected; #, $P < 0.03$; ##, $P < 0.05$. (G) IL-23 production by wild-type and *Batf2*$^{-/-}$ BMMφs. Data are mean ± SEM from three independent experiments. #, $P < 0.05$; ##, $P < 0.001$.

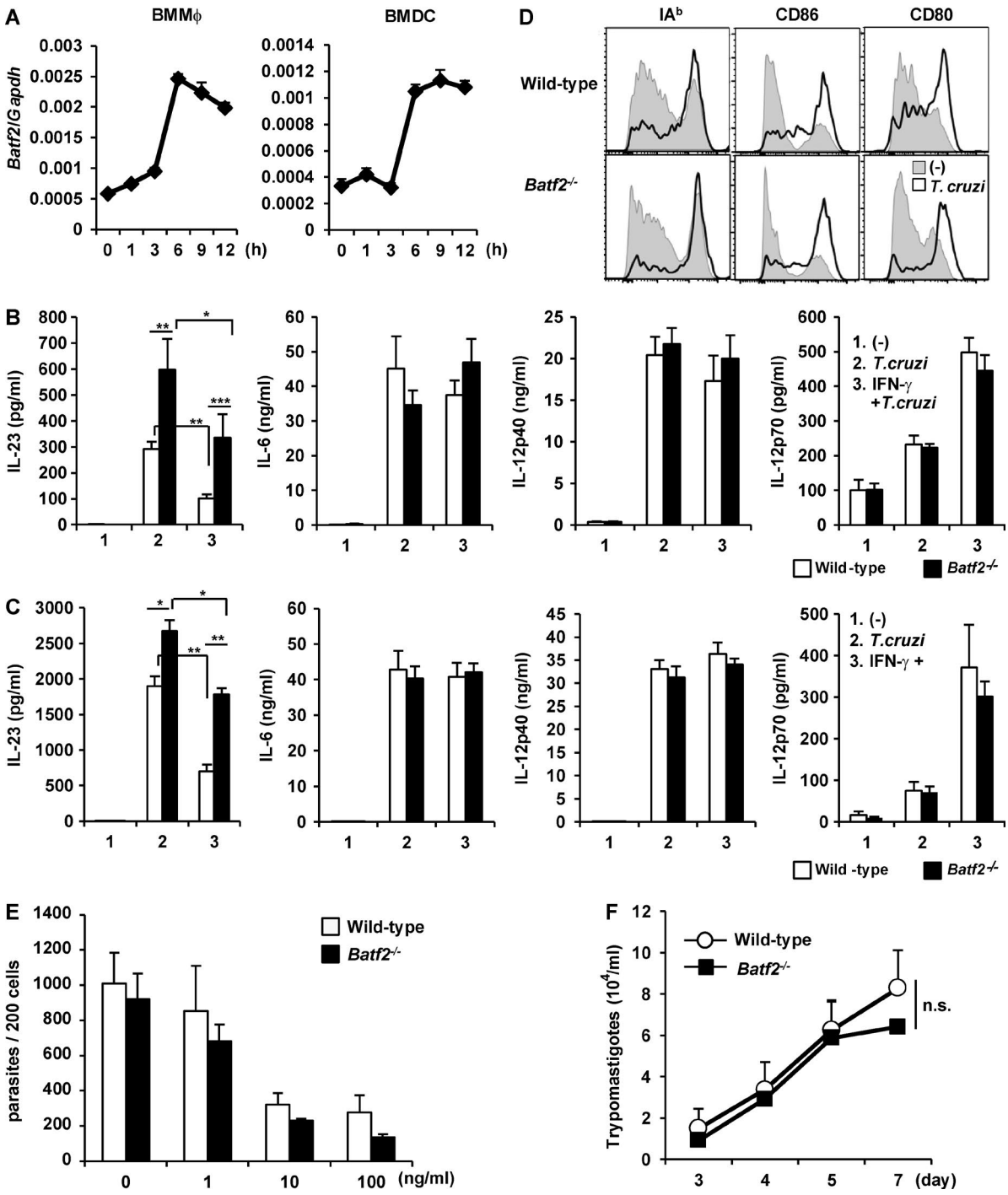

Figure 5. **Increased IL-23 production by *T. cruzi*–infected *Batf2*$^{-/-}$ innate immune cells.** (A) Expression of *Batf2* in BMMφs and BMDCs after *T. cruzi* infection. All data are representative of two independent experiments (mean values ± SD). (B and C) Production of IL-23, IL-12p40, IL-12p70, and IL-6 by *T. cruzi*–infected wild-type and *Batf2*$^{-/-}$ BMMφs (B) and BMDCs (C). Data are mean ± SEM from four independent experiments. *, $P < 0.05$; **, $P < 0.03$; ***, $P < 0.01$. (D) Surface expression of I-A^b, CD86, and CD80 on BMDCs after *T. cruzi* infection for 36 h. All data are representative of three independent experiments. (E) Parasite number per 200 BMMφs prepared from wild-type and *Batf2*$^{-/-}$ mice. (F) Numbers of trypomastigotes in the culture supernatants. (E and F) Graphs show the mean values ± SEM of three independent experiments. n.s., not significant.

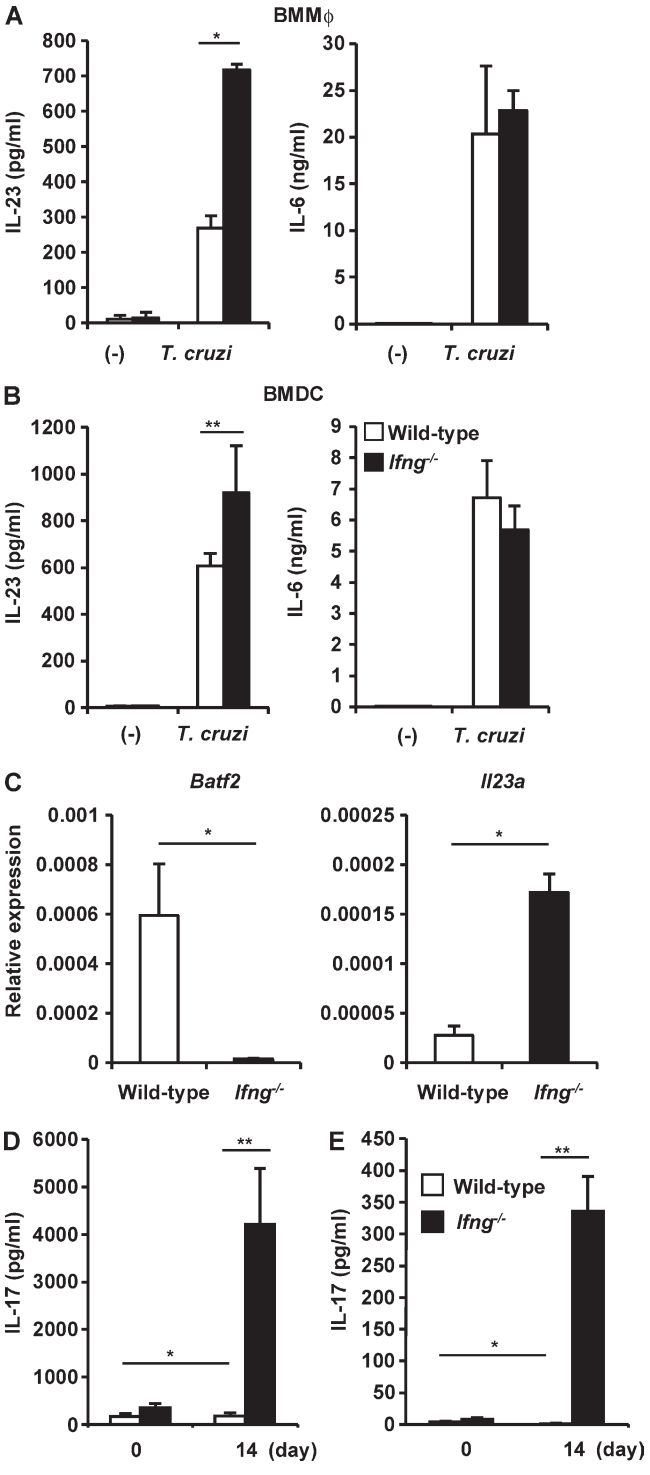

Figure 6. **Increased expression of *Il23a* in Mφs and Th17 responses in *T. cruzi*–infected *Ifng*$^{-/-}$ mice.** (A and B) Production of IL-23 and IL-6 by BMMφs (A) and BMDCs (B). Graphs show mean values ± SEM of four independent experiments. *, $P < 0.003$; **, $P < 0.05$. (C) Expression of *Batf2* and *Il23a* in CD11b$^+$ F4/80$^+$ Mφs from the spleens of wild-type and *Ifng*$^{-/-}$ mice 14 d after infection ($n = 3$ per group). Mean values ± SD. *, $P < 0.01$. (D and E) IL-17 production by CD4$^+$ T cells from the spleens of *T. cruzi*–infected mice ($n = 4$) or uninfected mice ($n = 3$) stimulated with anti-CD3 antibody (D) or freeze-thawed *T. cruzi* (E). Mean values ± SEM. *, $P < 0.05$; **, $P < 0.001$.

24 h. The culture supernatants were then analyzed for IL-23 and IL-6 (Fig. 6, A and B). *Ifng*$^{-/-}$ BMMφs showed markedly greater production of IL-23, but not IL-6, than wild-type cells. *Ifng*$^{-/-}$ BMDCs also released higher levels of IL-23 after *T. cruzi* infection than wild-type cells. CD11b$^+$ F4/80$^+$ Mφs isolated from the spleens of wild-type and *Ifng*$^{-/-}$ mice 14 d after *T. cruzi* infection were analyzed for the expression of *Batf2* and *Il23a* (Fig. 6 C). In the CD11b$^+$ F4/80$^+$ Mφs from the spleens of *Ifng*$^{-/-}$ mice, *Batf2* expression was severely reduced compared with that in the wild-type cells. However, the expression of *Il23a* was higher in the *Ifng*$^{-/-}$ Mφs than in the wild-type Mφs. IL-17 production by CD4$^+$ T cells isolated from the spleens of wild-type and *Ifng*$^{-/-}$ mice infected with or without *T. cruzi* was evaluated (Fig. 6, D and E). IL-17 production by CD4$^+$ T cells stimulated with anti-CD3 antibody was markedly higher in *Ifng*$^{-/-}$ mice at 14 d after infection than in wild-type mice (Fig. 6 D). Antigen-specific IL-17 production was also significantly higher in CD4$^+$ T cells from *Ifng*$^{-/-}$ mice than in those from wild-type mice (Fig. 6 E). These findings demonstrate that IFN-γ mediates the suppression of *Il23a* expression in innate immune cells and the down-regulation of IL-17 production by CD4$^+$ T cells during *T. cruzi* infection. Because Mφs IL-23 production and T cell IL-17 production were similarly increased in *Ifng*$^{-/-}$ and *Batf2*$^{-/-}$ mice, IFN-γ–induced BATF2 expression is supposed to be responsible for the suppression of the Th17 responses during *T. cruzi* infection.

To further determine whether the higher levels of IL-23 production in innate immune cells are involved in the enhanced Th17 responses in *T. cruzi*–infected *Batf2*$^{-/-}$ mice, we generated *Il23a*$^{-/-}$ mice by the Cas9/CRISPR-mediated genome editing (Fig. S5 A). BMMφs prepared from *Il23a*$^{-/-}$ mice did not produce IL-23 in response to LPS (Fig. S5 B), indicating the successful generation of *Il23a*$^{-/-}$ mice by the genome editing method. *Il23a*$^{-/-}$ mice were used for generation of *Batf2*$^{-/-}$*Il23a*$^{-/-}$ mice. Wild-type, *Batf2*$^{-/-}$, *Il23a*$^{-/-}$, and *Batf2*$^{-/-}$*Il23a*$^{-/-}$ mice were infected i.p. with *T. cruzi*. CD4$^+$ T cells isolated from their spleens 20 d after infection were analyzed for production of IFN-γ and IL-17 (Fig. 7, A–D). There was no difference in IFN-γ production by CD4$^+$ T cells stimulated with anti-CD3 antibody (Fig. 7 A) or with freeze-thawed *T. cruzi* in the presence of antigen-presenting cells (Fig. 7 B) between wild-type, *Batf2*$^{-/-}$, *Il23a*$^{-/-}$, and *Batf2*$^{-/-}$*Il23a*$^{-/-}$ mice. In contrast, introduction of *Il23a* deficiency into *Batf2*$^{-/-}$ mice drastically reduced IL-17 production by CD4$^+$ T cells stimulated with anti-CD3 antibody (Fig. 7 C). IL-17 production by *Batf2*$^{-/-}$*Il23a*$^{-/-}$ CD4$^+$ T cells stimulated with freeze-thawed *T. cruzi* was also dramatically reduced compared with that by *Batf2*$^{-/-}$ CD4$^+$ T cells (Fig. 7 D). In addition, expression of *Il17* and *Il22* was mark-

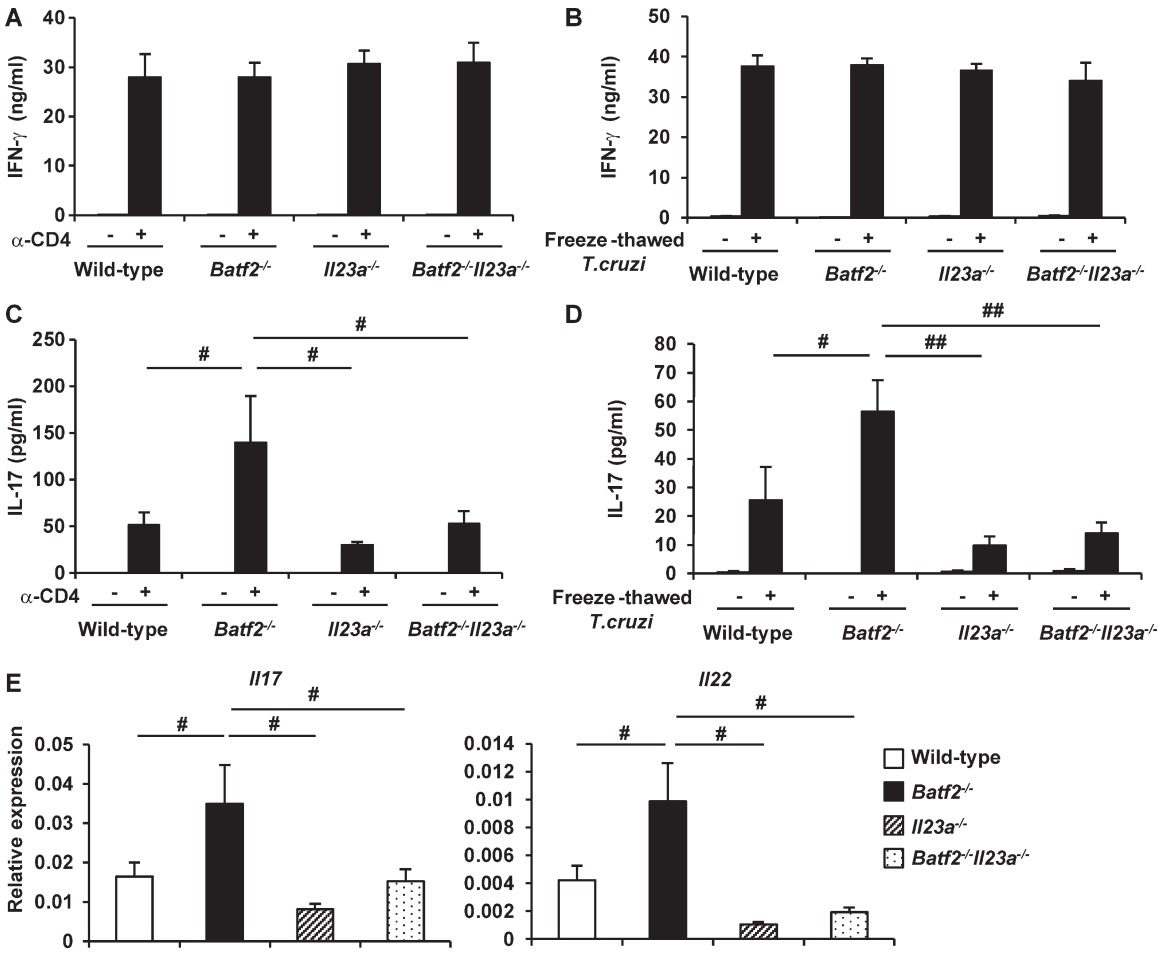

Figure 7. **Reduced CD4$^+$ T cell IL-17 production in *T. cruzi*–infected *Batf2*$^{-/-}$*Il23a*$^{-/-}$ mice.** (A–D) Wild-type (n = 18), *Batf2*$^{-/-}$ (n = 12), *Il23a*$^{-/-}$ (n = 9), and *Batf2*$^{-/-}$*Il23a*$^{-/-}$ (n = 9) mice were infected with *T. cruzi* for 20 d. CD4$^+$ T cells were isolated from the spleen of *T. cruzi*–infected mice and stimulated with anti-CD3 antibody (A and C) or freeze-thawed *T. cruzi* in the presence of antigen-presenting cells (B and D) for 24 h. The culture supernatants were analyzed for IFN-γ (A and B) and IL-17 (C and D) by ELISA. #, P < 0.045; ##, P < 0.006. (E) Expression of *Il17a* and *Il22* in CD4$^+$ T cells from the livers of *T. cruzi*–infected mice. #, P < 0.05. (A–E) Graphs show mean values ± SEM.

edly reduced in liver CD4$^+$ T cells from *T. cruzi*–infected *Batf2*$^{-/-}$*Il23a*$^{-/-}$ mice compared with those in *Batf2*$^{-/-}$ mice (Fig. 7 E). Furthermore, *Batf2*$^{-/-}$*Il23a*$^{-/-}$ mice exhibited increased parasite load in the livers, hearts, and blood compared with *Batf2*$^{-/-}$ mice (Fig. 8 A), but they showed reduced tissue damage after *T. cruzi* infection, as determined by lower pathological score and reduced serum or plasma concentration of AST, CK, and CRE (Fig. 8, B and C). These findings indicate that increased IL-23 production is responsible for the enhanced Th17 responses and immunopathology in *T. cruzi*–infected *Batf2*$^{-/-}$ mice.

Inhibition of *Il23a* expression by BATF2 through its interaction with c-JUN

We next investigated how BATF2 selectively down-regulates the expression of *Il23a* in innate immune cells. Because BATF2 does not contain a transcriptional activation domain, we suspected that it interacts with other transcription factors to regulate downstream genes. Upstream Regulator Analysis within Ingenuity Pathway Analysis (IPA) showed the indicated transcription factors as significantly enriched upstream regulators of the genes up-regulated in *Batf2*$^{-/-}$ BMMφs shown in Table S1 (Fig. 9 A). IPA was also used to determine the protein–protein interaction networks associated with BATF2. Among the molecules predicted to be upstream regulators of BATF2-dependent genes (Fig. 9 A), IPA showed that BATF2 binds to c-JUN, JUNB, and RELA/NF-κBp65 (Fig. S5 C). Therefore, we analyzed the interactions between BATF2 and these molecules with coimmunoprecipitation assays. HEK293 cells were cotransfected with Flag-BATF2 expression vector and c-JUN or JUNB expression vectors. TLR4-expressing HEK293 cells were transfected with Flag-BATF2 expression vector and stimulated with LPS to analyze the interaction between BATF2 and NF-κBp65. The cell lysates were immu-

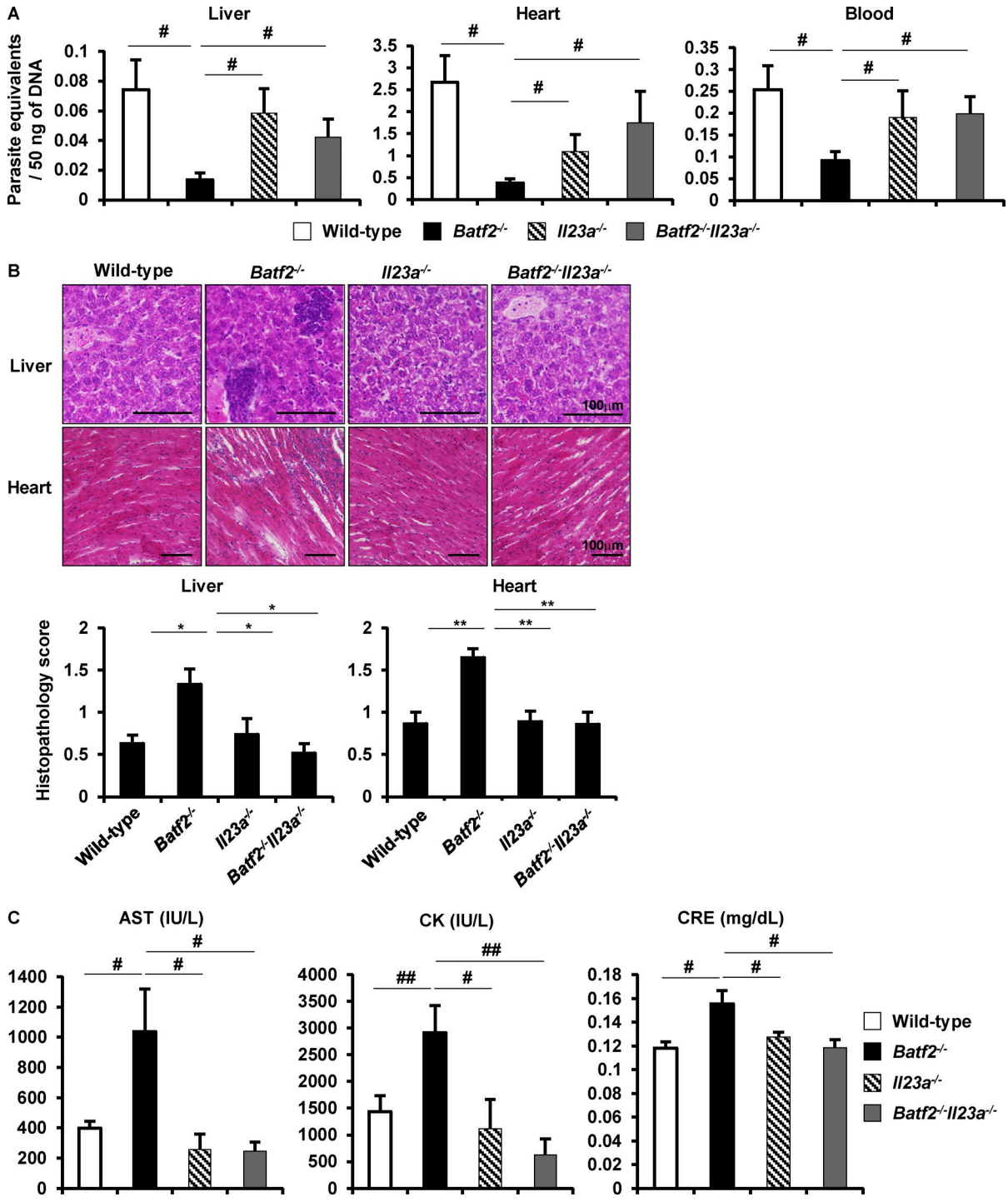

Figure 8. **IL-23–mediated immunopathology in *Batf2*$^{-/-}$ mice during *T. cruzi* infection.** (A) Parasite equivalents in the livers, hearts, and blood of *T. cruzi*–infected wild-type ($n = 18$), *Batf2*$^{-/-}$ ($n = 12$), *Il23a*$^{-/-}$ ($n = 9$), and *Batf2*$^{-/-}$*Il23a*$^{-/-}$ ($n = 9$) mice (mean values ± SEM). #, $P < 0.05$. (B) Representative sections (top) and pathological score (bottom) in *T. cruzi*–infected mice. Data are mean values ± SEM. Bars, 100 µm. *, $P < 0.009$; **, $P < 0.006$. (C) Concentrations of AST and CK in the plasma and CRE in the sera of *T. cruzi*–infected mice. Data are mean ± SEM. #, $P < 0.05$; ##, $P < 0.01$.

noprecipitated with anti-Flag antibody, and immunoblotting was performed with the indicated antibodies (Fig. S5, D–F). Among the three transcription factors, c-JUN and JUNB, but not NF-κBp65, interacted with BATF2. It has been shown that the heterodimer ATF-2/c-JUN, but not ATF-2/JUNB, drives the activity of the *Il23a* promoter (Liu et al., 2009).

Therefore, we analyzed whether BATF2 negatively regulates c-JUN–ATF-2 heterodimer-mediated activation of the *Il23a* promoter (Fig. 9 B). HEK293 cells were transfected with a pLuc vector containing the *Il23a* promoter region with or without BATF2, c-JUN, and ATF-2 expression vectors, and luciferase activity in the cell lysates was measured. The introduction of c-JUN and ATF-2 induced activation of the *Il23a* promoter. However, the expression of BATF2 inhibited the c-JUN–ATF-2 heterodimer–induced activity of *Il23a* promoter. To further clarify how BATF2 down-regulates c-JUN–ATF-2 heterodimer–dependent expression of *Il23a*, HEK293 cells were transfected with the Flag-BATF2 expression vector, with or without the c-JUN and ATF-2 expression vectors, and the cell lysates were immunoprecipitated with anti–c-JUN antibody. Immunoblotting was then performed with the indicated antibodies (Fig. 9 C). c-JUN interacted individually with BATF2 and ATF-2. However, in the presence of BATF2, c-JUN was associated with BATF2, but not with ATF-2. BATF2 lacking the leucine zipper motif (ΔBATF2), which contains the protein–protein interaction domain, was unable to suppress the LPS-induced *Il23a* promoter activity (Fig. 9 D). ΔBATF2 also did not interact with c-JUN (Fig. 9 E). When *Batf2*$^{-/-}$ BMMφs were transfected with a vector expressing full-length BATF2 or ΔBATF2, the full-length protein, but not ΔBATF2, suppressed LPS-induced *Il23a* expression (Fig. 9 F). We also investigated the effect of BATF2-mediated disruption of c-JUN/ATF2 heterodimer formation on the transcription of *Il23a*. In addition to innate immune cells, BATF2 was robustly induced by IFN-γ in MEFs (Fig. S5 G). Furthermore, expression of *Il23a* was higher in *Batf2*$^{-/-}$ MEFs stimulated with LPS after IFN-γ treatment than in wild-type MEFs (Fig. S5 H). In this context, chromatin immunoprecipitation (ChIP) analysis showed that only a little ATF-2 was instantaneously recruited at the AP-1–binding site in the *Il23a* promoter in IFN-γ–pretreated wild-type MEFs in response to LPS, whereas NF-κBp65 recruitment to the *Il23a* promoter was markedly increased, as previously described (Mise-Omata et al., 2007; Mühlbauer et al., 2008; Fig. 9 G and Fig. S5 I). In contrast, *Batf2*$^{-/-}$ MEFs showed increased levels of ATF2 and prolonged ATF-2 binding to the *Il23a* promoter after LPS stimulation (Fig. 9 G). These findings indicate that IFN-γ–inducible BATF2 inhibits the recruitment of the c-JUN–ATF-2 heterodimer to the *Il23a* promoter by preventing the formation of the c-JUN–ATF-2 complex when it directly interacts with c-JUN, leading to the suppression of *Il23a* expression.

DISCUSSION

In this study, we have demonstrated the mechanism underlying regulation of the IL-23–Th17 pathway by BATF2 during *T. cruzi* infection. IFN-γ–inducible BATF2 in innate immune cells suppressed IL-23 production by preventing the formation of the c-JUN–ATF-2 heterodimer, resulting in the inhibition of excessive Th17 responses during *T. cruzi* infection.

Compared with wild-type mice, *T. cruzi*–infected *Batf2*$^{-/-}$ mice showed lower mortality despite the development of severe immunopathology. Previous studies have shown that parasite-infected *Il27ra*$^{-/-}$ mice produced high amounts of IFN-γ and IL-17, with high mortality rates (Hamano et al., 2003; Villarino et al., 2003; Stumhofer et al., 2006; Findlay et al., 2010). However, treatment with anti–IFN-γ antibody alone dramatically reduced mortality (Hamano et al., 2003), indicating that excessive IL-17 is not implicated in the enhanced host lethality during *T. cruzi* infection. Therefore, increased IL-17 production in *Batf2*$^{-/-}$ mice might be associated with reduced parasite burden leading to low mortality, while inducing the severe immunopathology. In *Batf2*$^{-/-}$*Il23a*$^{-/-}$ mice, parasite number was partially reduced compared with that in wild-type mice, suggesting the possibility that BATF2-dependent genes other than *Il23a* also contribute to regulation of the parasite burden.

IL-17 promotes recruitment and activation of neutrophils (Kolaczkowska and Kubes, 2013). In accordance with the enhanced Th17 responses, a neutrophil-produced tissue damage factor, myeloperoxidase (Kolaczkowska and Kubes, 2013), was highly expressed in tissues of *T. cruzi*–infected *Batf2*$^{-/-}$ mice, suggesting that increased IL-23 production in *Batf2*$^{-/-}$ mice leads to neutrophil-related local tissue damage through enhanced IL-17 production. In the liver, *Il23a* is expressed in Kupffer cells and CD11c^{+} DCs (unpublished data), indicating that BATF2 might negatively regulate *Il23a* expression in these cells and thereby suppress immunopathological Th17 responses.

Multiple studies have identified several IL-17–producing cells besides Th17 cells, including invariant natural killer T cells, type 3 innate lymphoid cells, activated B cells, and innate γδ T cells (Cua and Tato, 2010; Bermejo et al., 2013). To determine whether CD4^{+} T cell–derived IL-17 is responsible for the multiorgan pathology in *Batf2*$^{-/-}$ mice, we attempted to deplete CD4^{+} T cells in *Batf2*$^{-/-}$ mice by intraperitoneally injecting with monoclonal anti-CD4 antibody after *T. cruzi* infection. However, effective depletion of CD4^{+} T cells in the livers and spleens could not be achieved, although CD4^{+} T cells in the peripheral blood severely decreased (unpublished data). Therefore, it would be an important future issue to characterize the IL-17–producing cells in detail during *T. cruzi* infection and to determine whether BATF2 controls IL-17 production in these cells by down-regulating *Il23a* expression in innate myeloid cells.

In the present study, *Ifng*$^{-/-}$ BMMφs and BMDCs showed higher *T. cruzi*–mediated IL-23 production than wild-type cells, indicating that BATF2, which is induced by IFN-γ autocrine signaling in innate immune cells, is responsible for the suppression of IL-23 production after *T. cruzi* infection. We also found that IFN-γ pretreatment leads to severely reduced IL-23 production in wild-type innate immune cells infected with *T. cruzi*, suggesting that BATF2 expression in innate myeloid cells is enhanced by potent IFN-γ producers in vivo, thereby restricting IL-23 production. However,

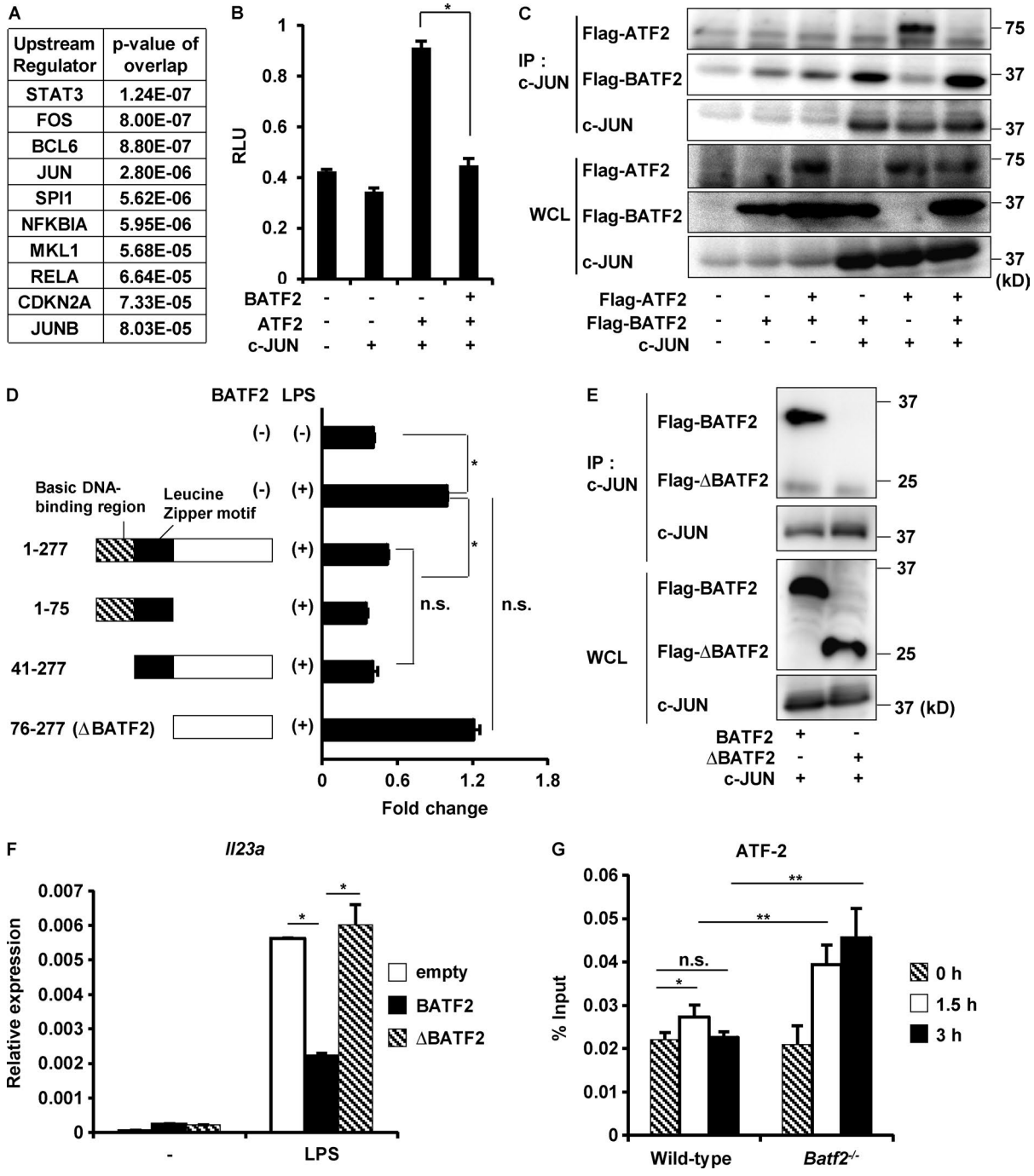

Figure 9. **BATF2 down-regulates *Il23a* expression through its interaction with c-JUN.** (A) Enrichment analysis of the upstream regulators of genes up-regulated in *Batf2*$^{-/-}$ BMMφs. (B) Luciferase activity of *Il23a* promoter. Data are representative of three independent experiments. Graph show mean values ± SD of triplicate wells. *, P < 0.001. RLU, relative light unit. (C) Coimmunoprecipitation (IP) assay with anti–c-JUN antibody for immunoprecipitation and the indicated antibodies for immunoblotting. WCL, whole cell lysate. (D) Luciferase activity of *Il23a* promoter in response to LPS. Data are representative of three independent experiments. Mean values ± SD for triplicate wells are shown. *, P < 0.01; n.s., not significant. (E) Coimmunoprecipitation assay with anti–c-JUN antibody for immunoprecipitation and the indicated antibodies for immunoblotting. (F) *Batf2*$^{-/-}$ BMMφs were transfected with the indicated vectors by nucleofection and, after 18 h, stimulated with LPS for 1 h, and their expression of *Il23a* was analyzed. Data are representative of three independent experiments. Graphs show mean values ± SD of triplicate measurements. *, P < 0.01. (G) ChIP assay for the *Il23a* promoter of AP-1–binding site was performed with anti–ATF-2 antibody using wild-type and *Batf2*$^{-/-}$ MEFs. Means ± SD of triplicate PCRs on identical samples. *, P < 0.03; **, P < 0.005; n.s., not significant. These values are representative of three independent experiments.

in *Batf2*$^{-/-}$ innate immune cells, IFN-γ-mediated reduction of IL-23 production was partially observed during *T. cruzi* infection and LPS stimulation. In this regard, it has been shown that IFN-γ depresses the recruitment of NF-κBp65 to the *Il23a* promoter by inducing histone modification in the early phase of the LPS responses (Sheikh et al., 2010). Therefore, it appears that IFN-γ suppresses *Il23a* expression in two ways during *T. cruzi* infection: IFN-γ induces both histone modification–mediated and BATF2-mediated reduction of *Il23a* expression. In *T. cruzi*–infected *Ifng*$^{-/-}$ mice, production of IL-17 by CD4^{+} T cells was markedly increased, as previously described (Cobb et al., 2010). IFN-γ–inducible T-bet is implicated in the suppression of Th17 cell differentiation by preventing the activation of RORγt (Lazarevic et al., 2011). Furthermore, IFN-γ acts on the histone modification of Th17-related transcription factors, including RORγt, STAT3, and STAT1 (Liu et al., 2015). In this study, we characterized a novel mechanism by which IFN-γ–inducible BATF2 contributes to the attenuation of the Th17 responses by down-regulating IL-23 production.

A previous study reported that BATF2 is responsible for the induction of *Tnf* and *Il12b* expression by interacting with IRF1 in LPS-stimulated BMMφs induced by L929 cell–conditioned medium (Roy et al., 2015). However, we observed no changes in *Tnf* or *Il12b* expression in IFN-γ plus LPS–stimulated *Batf2*$^{-/-}$ BMMφs, which were induced by GM-CSF. LPS-induced expression of *Tnf*, *Ccl5*, and *Nos2* was decreased in the absence of BATF2 when we prepared BMMφs using L929 cell–conditioned medium (unpublished data); however, these genes were normally induced in GM-CSF–induced *Batf2*$^{-/-}$ BMMφs (unpublished data). Thus, the discrepancy between the two studies may be explained by the polarization of Mφs because L929 cell–conditioned medium, containing high levels of M-CSF–induced BMMφs, is skewed to the M2Mφ phenotype, whereas GM-CSF-induced BMMφs is skewed to the M1Mφ phenotype. Therefore, BATF2 might regulate its downstream genes via Mφ type–specific mechanisms.

IL-27 suppresses tissue inflammation by inhibiting effector T cell responses and inducing IL-10–producing Tr1 cells during parasite infection (Hamano et al., 2003; Stumhofer et al., 2006; Hall et al., 2012). IL-27 production was slightly decreased in *Batf2*$^{-/-}$ BMMφs infected with *T. cruzi* (unpublished data). A modest reduction of IL-27 production in *Batf2*$^{-/-}$ BMMφs is not thought to be a major cause of the increased Th17 responses in *Batf2*$^{-/-}$ mice for the following reasons: (a) *T. cruzi*–infected *Batf2*$^{-/-}$ mice showed normal Th1 responses and IL-10–producing CD4^{+} T cell development; and (b) *T. cruzi*–infected *Batf2*$^{-/-}$*Il23a*$^{-/-}$ mice showed decreased IL-17 production by CD4^{+} T cells. IL-27 suppresses Th17 responses during the chronic phase of *T. gondii* infection (Stumhofer et al., 2006). Thus, it would be an important future issue to analyze the effects of BATF2-dependent regulation of IL-27 production on the chronic phase of *T. cruzi* infection.

In the present study, we have demonstrated that IFN-γ–inducible BATF2 exerts its immunoregulatory function through the suppression of *Il23a* by interacting directly with c-JUN in innate immune cells, thereby preventing immunopathological Th17 responses during *T. cruzi* infection. BATF2 is also broadly expressed in nonhematopoietic cells, such as vascular cells (Murphy et al., 2013; Chmielewski et al., 2014) and fibroblasts, as shown in the current study. Therefore, it would be interesting to evaluate the precise role of BATF2 during *T. cruzi* infection using innate myeloid cell–specific BATF2-deficient mice in a future study. In addition, enhanced intestinal IL-23 production and Th17 responses, which were associated with disturbed intestinal homeostasis, were observed in *Batf2*$^{-/-}$ mice (unpublished data). Thus, BATF2-mediated regulation of Th17 responses is not specific to *T. cruzi* infection, but is applicable to several models. Analyses of the involvement of BATF2 in other infectious models and Th17-mediated immune disorder models would be an interesting future issue.

MATERIALS AND METHODS

Mice

C57BL/6 mice were purchased from Japan SLC. *Ifng*$^{-/-}$ mice were generated as described previously (Tagawa et al., 1997). All mice were maintained under specific pathogen–free conditions. All animal experiments were conducted in accordance with the guidelines of the Animal Care and Use Committee of Osaka University.

Generation of *Batf2*$^{-/-}$ and *Il23a*$^{-/-}$ mice

To generate *Batf2*$^{-/-}$ mice, the targeted vector was constructed by replacing exon 3 of *Batf2* with a neomycin resistance gene cassette, and a gene encoding herpes simplex virus thymidine kinase driven by a phosphoglycerate kinase promoter was inserted into the genomic fragment for negative selection. After embryonic day 14, embryonic stem cells were transfected with the targeted vector, and colonies doubly resistance to G418 and ganciclovir were selected and screened with PCR and Southern blot analysis. Homologous recombinants were microinjected into blastocysts of female C57BL/6 mice, and the heterozygous F1 progeny were intercrossed to obtain *Batf2*-deficient mice. *Batf2*-deficient mice and their wild-type littermates from these intercrosses were confirmed with Southern blot analysis and real-time RT-PCR analysis and were used for subsequent experiments. *Batf2*-deficient mice were backcrossed to C57BL/6 mice for at least six generations, and *Batf2*-deficient mice and their wild-type littermates from the intercrosses of heterozygous mice were used for the experiments.

To generate *Il23a*$^{-/-}$ mice by the Cas9/CRISPR system, *Il23a*-gAS1-F (5′-CACCGCAGAGCAGTAATAATGCTA-3′) and *Il23a*-gAS1-R (5′-AAACTAGCATTATTACTG CTCTGC-3′) oligonucleotides and *Il23a*-gAS2-F (5′-CAC CCTGGAACGCACATGCACCAG-3′) and *Il23a*-gAS2-R (5′-AAACCTGGTGCATGTGCGTTCCAG-3′; Thermo Fisher Scientific) were annealed and inserted into the BbsI restriction site in the px330 vector (plasmid 42230; Addgene)

by Ligation high v. 2 (Toyobo). This plasmid was designated as px330-*Il23a*-gAS1 and px330-*Il23a*-gAS2, respectively. The px330-*Il23a*-gAS1 together with px330-*Il23a*-gAS2 vectors were injected into the pronuclei of one-cell-stage embryos from B6D2F1 mice. The eggs were cultivated in kSOM overnight and then transferred into the oviducts of pseudo-pregnant females.

Reagents

The Ca^{2+} ionophore A23187, PMA, LPS (O55: B5), and an anti-Flag antibody (clone M1) were purchased from Sigma-Aldrich. Anti-mouse c-JUN (clone H-79), JUNB (clone N-17), and NF-kBp65 (clone C-20) antibodies were purchased from Santa Cruz Biotechnology, Inc. Anti-ATF2 antibody (clone 20F1) was purchased from Cell Signaling Technology.

Preparation of Mφs and DCs

To prepare BMDCs and BMMφs, BM cells were prepared from mouse femurs and tibias, passed through a nylon mesh, and cultured in RPMI 1640 medium containing 10% FBS, 100 μM 2-mercaptoethanol, and 10 ng/ml GM-CSF (PeproTech). After 6 d, nonadherent cells were used as BMDCs, and adherent cells were used as BMMφs in the experiments. To isolate PECs, mice were injected i.p. with 2 ml of 4% thioglycolate medium (Sigma-Aldrich), and cells in the peritoneal exudate were isolated from the peritoneal cavity 3 d after injection. The cells were incubated for 2 h and then washed three times with HBSS. The remaining adherent cells were used as PECs in the experiments.

Parasite and experimental infection

The *T. cruzi* Tulahuen strain was maintained in vitro in LLC-MK_2 cells, with passage every 3 d. For the in vitro experiments, 5×10^5 Mφs or DCs were infected with 2.5×10^6 *T. cruzi*. For the in vivo experiments, the mice were injected i.p. with 5×10^2 *T. cruzi*.

Flow cytometry

The following antibodies were purchased from BD: anti–mouse-CD16/32 (2.4.G2), APC-conjugated anti-CD11c (clone HL3), PE-conjugated anti-CD103 (clone M290), PE-Cy7–conjugated anti–Ly-6C (clone AL-21), FITC-conjugated anti–Ly-6G (clone 1A8), biotin-conjugated anti-IA^b (AF6-120.1), PE-conjugated anti-CD80 (B7-1), and streptavidin-APC antibodies. Pacific blue–conjugated anti-CD11b (clone M1/70), Percp-Cy5.5–conjugated anti-CD4 (clone CK1.5), APC-conjugated anti-CD8 (clone 53–6.7), PE-conjugated anti-CD19 (clone 6D5), APC-conjugated anti–IL-17A (TC11-18H10.1), APC-conjugated anti-F4/80 (BM8), FITC-conjugated anti–IFN-γ (clone XMG1.2), and PE-conjugated anti–IL-10 (JES5-16E3) antibodies were purchased from BioLegend. FITC-conjugated anti-CD86 antibody (clone GL1) was purchased from eBioscience. Flow cytometric analysis was performed with a FACSCanto II flow cytometer (BD) with FlowJo software (Tree Star). $CD11b^+$ $F4/80^+$ Mφs from the spleens of *T. cruzi*–infected mice were isolated with a FACSAria flow cytometer (BD). The instrumental compensation was set in each experiment using single-color, two-color, or four-color stained samples.

Real-time RT-PCR

$CD4^+$ T cells isolated from the spleens and livers after *T. cruzi* infection for 20 d were stimulated with 50 ng/ml PMA and 5 μM calcium ionophore A23187 for 2 h, and total RNA was isolated. PECs, BMMφs, and BMDCs were pretreated with IFN-γ for 4 h and stimulated with LPS for the indicated periods, and total RNA was isolated. Total RNA was isolated using the RNeasy Mini kit (QIAGEN), and 1–2 μg of RNA was reverse transcribed with Moloney Murine Leukemia Virus Reverse transcription (Promega) and random primers (Toyobo) after treatment with RQ1 DNase I (Promega). Real-time RT-PCR was performed on a Step One Plus Real-Time PCR System (Applied Biosystems) using GoTaq qPCR Master Mix (Promega). All values were normalized to the expression of *Gapdh*, encoding glyceraldhyde-3-phosphate dehydrogenase, and the fold difference in expression relative to that of *Gapdh* is shown. The amplification conditions were as follows: 50°C (2 min), 95°C (10 min), and 40 cycles of 95°C (15 s) and 60°C (60 s). The following primer sets were used: *Gapdh*, 5′-CCTCGTCCCGTAGACAAAATG-3′ and 5′-TCTCCACTTTGCCACTGCAA-3′; *Batf*, 5′-AGACACAGAAAGCCGACACC-3′ and 5′-TCAGCACTGATGTGAAGTAC-3′; *Batf2*, 5′-GCCCAGCGCAGCCGGCAGAA-3′ and 5′-CCAGCTCAGTCTGCAAGGCCT-3′; *Batf3*, 5′-AAGGACGATGACAGGAAAG-3′ and 5′-CTCTCGTGCTCCTCGTGGAG-3′; *Cd86*, 5′-TACGGAAGCACCCACGATGG-3′ and 5′-AATAAGCTTGCGTCTCCACG-3′; *Fgl2*, 5′-AGTGTCCCAGCCAAGAACAC-3′ and 5′-GATCAGGGGTAACTCTGTAG-3′; *Gbp7*, 5′-TGAGAGAGCAAGAGGTGAAGCTG-3′ and 5′-ACTTACCAGAACCAGGCACTAC-3′; *Gbp8*, 5′-CCACAATGAAACATCTGTCCGTGAACC-3′ and 5′-CCAGAGGGAAACCGTGATTCTGTC-3′; *Ifng*, 5′-TCAAGTGGCATAGATGTGGAAGAA-3′ and 5′-TGGCTCTGCAGGATTTTCATG-3′; *Irf1*, 5′-CCGAAGACCTTATGAAGCTCTTTG-3′ and 5′-GCAAGTATCCCTTGCCATCG-3′; *Il10*, 5′-CTGGGTGAGAAGCTGAAGACC-3′ and 5′-CATGGCCTTGTAGACACCTTG-3′; *Il12b*, 5′-GGTTTGCCATCGTTTGCTGG-3′ and 5′-CATCTTCTTCAGGCGTGTCAC-3′; *Il12rb1*, 5′-CCTGCTTTGCCAGCTAGGCG-3′ and 5′-CCTGGGTCCTAAGGGTGAGC-3′; *Il17a*, 5′-GGACTCTCCACCGCAATGA-3′ and 5′-GGCACTGAGCTTCCCAGATC-3′; *Il6*, 5′-CTGCAAGAGACTTCCATCCAGTT-3′ and 5′-AAGTAGGGAAGGCCGTGGTT-3′; *Il22*, 5′-TGATGGCTGTCCTGCAGAAA-3′ and 5′-CAGCTGGCGGCAAAG-3′; *Il23a*, 5′-CCAGCAGCTCTCTCGGAATCT-3′ and 5′-ACTGCTGACTAGAACTCAGGC-3′; *Irgm*, 5′-AATAAAACCAGAGAGCCTCA-3′ and 5′-TAATGGGTCTCTGCCATGTT-3′; *Mpo*, 5′-ATCACGGCCTCCCAGGATACAATG-3′ and

5′-ACCGCCCATCCAGATGTCAAT-3′; *Stat1*, 5′-GCG TGCAGTGAGTGAGTGAG-3′ and 5′-CAACACAAG CAATCACCACA-3′; *Tnfa* 5′-TCCAGGCGGTGCCTA TGT-3′ and 5′-CACCCCGAAGTTCAGTAGACAGA-3′; and *Csf2*, 5′-TCGAGCAGGGTCTACGGGGC-3′ and 5′-TCCGTTTCCGGAGTTGGGGG-3′.

Cytokine analysis

$CD4^+$ T cells were isolated from the spleens and livers of mice on the indicated days after *T. cruzi* infection with MACS technology (Miltenyi Biotec) and stimulated with anti-CD3 antibody or freeze-thawed *T. cruzi* in the presence of antigen-presenting cells in a 1:1:1 ratio for 24 h. PECs, BMMφs, and BMDCs were pretreated with 10 ng/ml IFN-γ and stimulated with 100 ng/ml LPS for 24 h. BMMφs and BMDCs pretreated with or without 10 ng/ml IFN-γ for 4 h were thoroughly washed and infected with *T. cruzi* in a ratio of 1:5 and cultured for 24 h. The concentrations of IL-17, IFN-γ, IL-23, TNF, IL-12p40, IL-12p70, and IL-6 in the culture supernatants were measured with the Cytometric Bead Array kit (BD).

Intracellular cytokine staining

$CD4^+$ T cell intracellular IFN-γ, IL-10, and IL-17A expression was analyzed with a Cytofix/Cytoperm Plus kit with GolgiStop (BD), according to the manufacturer's instructions. In brief, $CD4^+$ T cells were incubated with 50 ng/ml PMA, 5 µM calcium ionophore A23187, and GolgiStop in complete RPMI 1640 at 37°C for 4 h. Surface staining was performed with anti-CD4 antibody for 20 min at 4°C, and intracellular cytokine staining was performed with anti–IL-17A, anti–IL-10, and anti–IFN-γ antibodies for 20 min.

T. cruzi killing assay

Wild-type and *Batf2*$^{-/-}$ BMMφs were pretreated with or without the indicated concentration of IFN-γ for 18 h, rigorously washed, and then infected with *T. cruzi* for 6 h. After washing, the cells were cultured for 72 h and fixed. After staining with Diff-Quik (Sysmex), the intracellular parasites were counted.

Luciferase assay

HEK293 cells were transfected with the indicated expression plasmids together with the reporter plasmid *Il23a*–Luc and the internal control plasmid phRG-TK. After 12 h, luciferase activities of the whole cell lysates were measured with the Dual-Luciferase Reporter Assay System (Promega) and a Lumat LB 9507 luminometer (Berthold Technologies). TLR4-expressing HEK293 cells were transfected with the plasmids. After 12 h, the cells were stimulated with 100 ng/ml LPS for 24 h, lysed, and then measured with the Dual-Luciferase Reporter Assay System.

Transfection into BMMφs

Batf2$^{-/-}$ BMMφs were transfected with pcDNA3 containing the full-length form of BATF2 or the mutant form which the leucine zipper motif had been deleted, using nucleofection (Nucleofector kit for Mouse Macrophages; Lonza). After 12 h, the cells were stimulated with 100 ng/ml LPS for 3 h, and then the expression of *Il23a* was analyzed.

RNA-seq analysis

Wild-type and *Batf2*$^{-/-}$ BMMφs pretreated with 10 ng/ml IFN-γ for 4 h were stimulated with (designated WT_3 and KO_3, respectively) or without (designated WT_0 and KO_0, respectively) 100 ng/ml LPS for 3 h. Total RNAs were extracted from the cells with RNeasy Mini kit (QIAGEN), according to the manufacturer's protocol. The libraries were constructed and sequenced at Kazusa DNA Research Institute (Chiba, Japan) using a SureSelect Strand-Specific RNA Library Prep kit (Agilent Technologies), according to the manufacturer's instructions. Sequencing was performed on an Illumina HiSeq 2000 sequencer with a TruSeq Rapid SBS kit v3 HS (Illumina) in the 50-base single-end mode. Illumina Casava 1.8.2 software was used for base calling. The low-quality regions of the raw reads were trimmed with Btrim. The sequenced reads were mapped to the mouse reference genome sequence (mm9) using TopHat v2.0.12. The fragments per kilobase of exons per million mapped fragments (FPKMs) were calculated using Cufflinks v2.1.1. Among the calculated genes with a normalized FPKM value >1.0 in WT_3, 98 genes were up-regulated >1.5-fold from WT_0 to WT_3 and >2.0-fold from WT_3 to KO_3 (Table S1). These results have been deposited in the National Center Biotechnology Information Gene Expression Omnibus database (GSE81724).

Quantitation of *T. cruzi* in tissues

The parasite load in the tissue was analyzed as previously described (Cencig et al., 2011; Caldas et al., 2012). In brief, concentrations of DNA purified from the liver, heart, and blood of *T. cruzi*–infected mice were adjusted to 25 ng/µl. Each PCR reaction was performed with 50 ng of genomic tissue DNA. The amount of tissue in each PCR was normalized to mouse TNF DNA (Cencig et al., 2011). *T. cruzi* standard curves were generated as previously described (Caldas et al., 2012). qPCR was performed on the Step One Plus Real-Time PCR System (Applied Biosystems) using GoTaq qPCR Master Mix (Promega). The amplification conditions were as follows: 95°C for 10 min, 40 cycles of 94°C for 15 s, and 64.3°C for 1 min. The following primer sets were used: *T. cruzi* specific primers, 5′-CGAGCTGTTGCCCACACG GGTGCT-3′ and 5′-CCTCCAAGCAGCGGATAGTTC AGG-3′ (Cencig et al., 2011); and *Tnf* primers, 5′-TCCCTC TCATCAGTTCTATGGCCCA-3′ and 5′-CAGCAAGCA TCTATGCACTTAGACCCC-3′ (Caldas et al., 2012).

Histopathological analysis

The livers and hearts collected from the mice 49 d after *T. cruzi* infection were fixed in 4% PFA. Paraffin-embedded 5-µm sections mounted on glass slides were stained with he-

matoxylin and eosin (H&E) and examined for histopathology with inflammatory cell infiltrates using light microcopy. Each section of the hearts (Leon et al., 2003) and livers (Barreto-de-Albuquerque et al., 2015) was evaluated for inflammation scores as previously described.

ChIP assay

The ChIP assay was performed as previously described, with modifications (Kayama et al., 2008). In brief, MEFs were stimulated with 100 ng/ml LPS for the indicated periods after treatment with 10 ng/ml IFN-γ for 5 h. The chromatin was cross-linked with 1% formaldehyde at room temperature for 10 min. The MEFs were washed with PBS, scraped, and then centrifuged at 800 *g*. The pellet was resuspended in SDS buffer supplemented with protease inhibitor. The chromatin was sonicated 15 times with 30 s pulses, centrifuged at 1,300 *g* to remove any debris, diluted fivefold with ChIP dilution buffer, and precleared with salmon sperm DNA/protein A agarose (EMD Millipore). The diluted chromatin was immunoprecipitated at 4°C overnight. The immune complexes were adsorbed onto salmon sperm DNA/protein A agarose beads, and washed once each with low-salt buffer, high-salt buffer, and LiCl buffer, and then twice with TE buffer. The immune complexes were extracted in elution buffer and incubated for 4 h at 65°C. The DNA was then extracted by incubating it in proteinase K buffer for 1 h at 45°C. The purified DNA was used in qPCR, using 10% of each input as the standard. The *Il23a* promoter-specific primer was designed to include the NF-κB–binding site or AP-1–binding site. The primer sequences were as follows: NF-κB–binding site, 5′-TGGCCTCACTCTGAC GTCCA-3′ and 5′-GTAACACCCAGGGAAGCAGC-3′; AP-1–binding site, 5′-AATCCCACCTGCTCTGAG TC-3′ and 5′-GTAGTCCGACTTCTAAGCGG-3′.

Statistical analysis

Differences between the control and experimental groups were evaluated with Student's *t* test. Differences of $P < 0.05$ were considered to be significant.

Online supplemental material

Fig. S1 shows the targeting construct for *Batf2*$^{-/-}$ mice, expression patterns of IFN-γ–dependent genes, and innate immune cell population of wild-type and *Batf2*$^{-/-}$ mice. Fig. S2 shows flow cytometric dot plots of cytokine-producing CD4$^+$ T cells of *T. cruzi*–infected mice. Fig. S3 displays production of IFN-γ and IL-17 in wild-type and *Batf2*$^{-/-}$ naive CD4$^+$ T cells cultured under Th0, Th1, and Th17 conditions. Fig. S4 shows cytokine production by wild-type and *Batf2*$^{-/-}$ PECs, BMMφs, and BMDCs. Fig. S5 shows the Cas9/gRNA-targeting site for *Il23a* and the analysis of BATF2-binding partners. Table S1, included in a separate Excel file, lists genes upregulated in response to LPS in *Batf2*$^{-/-}$ BMMφs pretreated with IFN-γ.

ACKNOWLEDGMENTS

We thank S. Nishioka, T. Kondo, and Y. Magota for their technical assistance; S. Pareek for critical reading of the manuscript; and C. Hidaka for secretarial assistance.

This work was supported by grants from the Ministry of Education, Culture, Sports, Science and Technology of Japan and the Japan Agency for Medical Research and Development (grant 15gm011002h0006; to K. Takeda) and by the Ichiro Kanehara Foundation for the Promotion of Medical Sciences and Medical Care and the Kurata Memorial Hitachi Science and Technology Foundation (to H. Kayama).

The authors declare no competing financial interests.

Author contributions: S. Kitada, H. Kayama, R. Koga, and M. Kobayashi designed and performed the experiments, analyzed the data, and revised the manuscript. D. Okuzaki designed the experiments, analyzed data, and supervised the RNA-seq analysis. A. Kumanogoh and M. Ikawa supervised the generation of Il23a$^{-/-}$ mice by the Cas9/CRISPR system. Y. Arima and M. Murakami analyzed the Ifng$^{-/-}$ mice. K. Takeda supervised the study, designed the experiments, analyzed the data, and wrote the manuscript.

Submitted: 11 July 2016
Revised: 8 December 2016
Accepted: 7 February 2017

REFERENCES

Ahern, P.P., C. Schiering, S. Buonocore, M.J. McGeachy, D.J. Cua, K.J. Maloy, and F. Powrie. 2010. Interleukin-23 drives intestinal inflammation through direct activity on T cells. *Immunity.* 33:279–288. http://dx.doi.org/10.1016/j.immuni.2010.08.010

Barreto-de-Albuquerque, J., D. Silva-dos-Santos, A.R. Pérez, L.R. Berbert, E. de Santana-van-Vliet, D.A. Farias-de-Oliveira, O.C. Moreira, E. Roggero, C.E. de Carvalho-Pinto, J. Jurberg, et al. 2015. *Trypanosoma cruzi* infection through the oral route promotes a severe infection in mice: New disease form from an old infection? *PLoS Negl. Trop. Dis.* 9:e0003849. http://dx.doi.org/10.1371/journal.pntd.0003849

Bermejo, D.A., S.W. Jackson, M. Gorosito-Serran, E.V. Acosta-Rodriguez, M.C. Amezcua-Vesely, B.D. Sather, A.K. Singh, S. Khim, J. Mucci, D. Liggitt, et al. 2013. *Trypanosoma cruzi* trans-sialidase initiates a program independent of the transcription factors RORγt and Ahr that leads to IL-17 production by activated B cells. *Nat. Immunol.* 14:514–522. http://dx.doi.org/10.1038/ni.2569

Bonney, K.M., J.M. Taylor, E.B. Thorp, C.L. Epting, and D.M. Engman. 2015. Depletion of regulatory T cells decreases cardiac parasitosis and inflammation in experimental Chagas disease. *Parasitol. Res.* 114:1167–1178. http://dx.doi.org/10.1007/s00436-014-4300-3

Caldas, S., I.S. Caldas, L.F. Diniz, W.G. Lima, R.P. Oliveira, A.B. Cecílio, I. Ribeiro, A. Talvani, and M.T. Bahia. 2012. Real-time PCR strategy for parasite quantification in blood and tissue samples of experimental *Trypanosoma cruzi* infection. *Acta Trop.* 123:170–177. http://dx.doi.org/10.1016/j.actatropica.2012.05.002

Cencig, S., N. Coltel, C. Truyens, and Y. Carlier. 2011. Parasitic loads in tissues of mice infected with *Trypanosoma cruzi* and treated with AmBisome. *PLoS Negl. Trop. Dis.* 5:e1216. http://dx.doi.org/10.1371/journal.pntd.0001216

Chmielewski, S., A. Olejnik, K. Sikorski, J. Pelisek, K. Błaszczyk, C. Aoqui, H. Nowicka, A. Zernecke, U. Heemann, J. Wesoly, et al. 2014. STAT1-dependent signal integration between IFNγ and TLR4 in vascular cells reflect pro-atherogenic responses in human atherosclerosis. *PLoS One.* 9:e113318. http://dx.doi.org/10.1371/journal.pone.0113318

Cobb, D., and R.B. Smeltz. 2012. Regulation of proinflammatory Th17 responses during *Trypanosoma cruzi* infection by IL-12 family cytokines. *J. Immunol.* 188:3766–3773. http://dx.doi.org/10.4049/jimmunol.1103478

Cobb, D., D. Hambright, and R.B. Smeltz. 2010. T-bet-independent effects of IL-12 family cytokines on regulation of Th17 responses to experimental

T. cruzi infection. *J. Leukoc. Biol.* 88:965–971. http://dx.doi.org/10.1189/jlb.0410238

Cua, D.J., and C.M. Tato. 2010. Innate IL-17-producing cells: The sentinels of the immune system. *Nat. Rev. Immunol.* 10:479–489. http://dx.doi.org/10.1038/nri2800

da Matta Guedes, P.M., F.R. Gutierrez, F.L. Maia, C.M. Milanezi, G.K. Silva, W.R. Pavanelli, and J.S. Silva. 2010. IL-17 produced during *Trypanosoma cruzi* infection plays a central role in regulating parasite-induced myocarditis. *PLoS Negl. Trop. Dis.* 4:e604. http://dx.doi.org/10.1371/journal.pntd.0000604

Erdmann, H., C. Roßnagel, J. Böhme, Y. Iwakura, T. Jacobs, U.E. Schaible, and C. Hölscher. 2013. IL-17A promotes macrophage effector mechanisms against *Trypanosoma cruzi* by trapping parasites in the endolysosomal compartment. *Immunobiology.* 218:910–923. http://dx.doi.org/10.1016/j.imbio.2012.10.005

Findlay, E.G., R. Greig, J.S. Stumhofer, J.C. Hafalla, J.B. de Souza, C.J. Saris, C.A. Hunter, E.M. Riley, and K.N. Couper. 2010. Essential role for IL-27 receptor signaling in prevention of Th1-mediated immunopathology during malaria infection. *J. Immunol.* 185:2482–2492. http://dx.doi.org/10.4049/jimmunol.0904019

Gaffen, S.L., R. Jain, A.V. Garg, and D.J. Cua. 2014. The IL-23-IL-17 immune axis: From mechanisms to therapeutic testing. *Nat. Rev. Immunol.* 14:585–600. http://dx.doi.org/10.1038/nri3707

Gazzinelli, R.T., and E.Y. Denkers. 2006. Protozoan encounters with Toll-like receptor signalling pathways: Implications for host parasitism. *Nat. Rev. Immunol.* 6:895–906. http://dx.doi.org/10.1038/nri1978

Guo, S., D. Cobb, and R.B. Smeltz. 2009. T-bet inhibits the in vivo differentiation of parasite-specific CD4+ Th17 cells in a T cell-intrinsic manner. *J. Immunol.* 182:6179–6186. http://dx.doi.org/10.4049/jimmunol.0803821

Hall, A.O., D.P. Beiting, C. Tato, B. John, G. Oldenhove, C.G. Lombana, G.H. Pritchard, J.S. Silver, N. Bouladoux, J.S. Stumhofer, et al. 2012. The cytokines interleukin 27 and interferon-γ promote distinct Treg cell populations required to limit infection-induced pathology. *Immunity.* 37:511–523. http://dx.doi.org/10.1016/j.immuni.2012.06.014

Hamano, S., K. Himeno, Y. Miyazaki, K. Ishii, A. Yamanaka, A. Takeda, M. Zhang, H. Hisaeda, T.W. Mak, A. Yoshimura, and H. Yoshida. 2003. WSX-1 is required for resistance to *Trypanosoma cruzi* infection by regulation of proinflammatory cytokine production. *Immunity.* 19:657–667. http://dx.doi.org/10.1016/S1074-7613(03)00298-X

Kawai, T., and S. Akira. 2011. Toll-like receptors and their crosstalk with other innate receptors in infection and immunity. *Immunity.* 34:637–650. http://dx.doi.org/10.1016/j.immuni.2011.05.006

Kayama, H., and K. Takeda. 2010. The innate immune response to *Trypanosoma cruzi* infection. *Microbes Infect.* 12:511–517. http://dx.doi.org/10.1016/j.micinf.2010.03.005

Kayama, H., V.R. Ramirez-Carrozzi, M. Yamamoto, T. Mizutani, H. Kuwata, H. Iba, M. Matsumoto, K. Honda, S.T. Smale, and K. Takeda. 2008. Class-specific regulation of pro-inflammatory genes by MyD88 pathways and IκBζ. *J. Biol. Chem.* 283:12468–12477 (published errata appear in *J. Biol. Chem.* 2015. 290:4815 and 22446). http://dx.doi.org/10.1074/jbc.M709965200

Kayama, H., R. Koga, K. Atarashi, M. Okuyama, T. Kimura, T.W. Mak, S. Uematsu, S. Akira, H. Takayanagi, K. Honda, et al. 2009. NFATc1 mediates Toll-like receptor-independent innate immune responses during *Trypanosoma cruzi* infection. *PLoS Pathog.* 5:e1000514. http://dx.doi.org/10.1371/journal.ppat.1000514

Kolaczkowska, E., and P. Kubes. 2013. Neutrophil recruitment and function in health and inflammation. *Nat. Rev. Immunol.* 13:159–175. http://dx.doi.org/10.1038/nri3399

Lazarevic, V., X. Chen, J.H. Shim, E.S. Hwang, E. Jang, A.N. Bolm, M. Oukka, V.K. Kuchroo, and L.H. Glimcher. 2011. T-bet represses T_H17 differentiation by preventing Runx1-mediated activation of the gene encoding RORγt. *Nat. Immunol.* 12:96–104. http://dx.doi.org/10.1038/ni.1969

Leon, J.S., K. Wang, and D.M. Engman. 2003. Captopril ameliorates myocarditis in acute experimental Chagas disease. *Circulation.* 107:2264–2269. http://dx.doi.org/10.1161/01.CIR.0000062690.79456.D0

Liu, W., X. Ouyang, J. Yang, J. Liu, Q. Li, Y. Gu, M. Fukata, T. Lin, J.C. He, M. Abreu, et al. 2009. AP-1 activated by Toll-like receptors regulates expression of IL-23 p19. *J. Biol. Chem.* 284:24006–24016. http://dx.doi.org/10.1074/jbc.M109.025528

Liu, X., S. Ren, X. Qu, C. Ge, K. Cheng, and R.C. Zhao. 2015. Mesenchymal stem cells inhibit Th17 cells differentiation via IFN-γ-mediated SOCS3 activation. *Immunol. Res.* 61:219–229. http://dx.doi.org/10.1007/s12026-014-8612-2

McGeachy, M.J., and S.J. McSorley. 2012. Microbial-induced Th17: Superhero or supervillain? *J. Immunol.* 189:3285–3291. http://dx.doi.org/10.4049/jimmunol.1201834

McGeachy, M.J., Y. Chen, C.M. Tato, A. Laurence, B. Joyce-Shaikh, W.M. Blumenschein, T.K. McClanahan, J.J. O'Shea, and D.J. Cua. 2009. The interleukin 23 receptor is essential for the terminal differentiation of interleukin 17-producing effector T helper cells in vivo. *Nat. Immunol.* 10:314–324. http://dx.doi.org/10.1038/ni.1698

Mise-Omata, S., E. Kuroda, J. Niikura, U. Yamashita, Y. Obata, and T.S. Doi. 2007. A proximal kappaB site in the IL-23 p19 promoter is responsible for RelA- and c-Rel-dependent transcription. *J. Immunol.* 179:6596–6603. http://dx.doi.org/10.4049/jimmunol.179.10.6596

Miyazaki, Y., S. Hamano, S. Wang, Y. Shimanoe, Y. Iwakura, and H. Yoshida. 2010. IL-17 is necessary for host protection against acute-phase *Trypanosoma cruzi* infection. *J. Immunol.* 185:1150–1157. http://dx.doi.org/10.4049/jimmunol.0900047

Mühlbauer, M., P.M. Chilton, T.C. Mitchell, and C. Jobin. 2008. Impaired Bcl3 up-regulation leads to enhanced lipopolysaccharide-induced interleukin (IL)-23P19 gene expression in IL-10(-/-) mice. *J. Biol. Chem.* 283:14182–14189. http://dx.doi.org/10.1074/jbc.M709029200

Murphy, T.L., R. Tussiwand, and K.M. Murphy. 2013. Specificity through cooperation: BATF-IRF interactions control immune-regulatory networks. *Nat. Rev. Immunol.* 13:499–509. http://dx.doi.org/10.1038/nri3470

Rangachari, M., N. Mauermann, R.R. Marty, S. Dirnhofer, M.O. Kurrer, V. Komnenovic, J.M. Penninger, and U. Eriksson. 2006. T-bet negatively regulates autoimmune myocarditis by suppressing local production of interleukin 17. *J. Exp. Med.* 203:2009–2019. http://dx.doi.org/10.1084/jem.20052222

Rodrigues, M.M., A.C. Oliveira, and M. Bellio. 2012. The immune response to *Trypanosoma cruzi*: Role of Toll-like receptors and perspectives for vaccine development. *J. Parasitol. Res.* 2012:507874. http://dx.doi.org/10.1155/2012/507874

Roy, S., R. Guler, S.P. Parihar, S. Schmeier, B. Kaczkowski, H. Nishimura, J.W. Shin, Y. Negishi, M. Ozturk, R. Hurdayal, et al. 2015. Batf2/Irf1 induces inflammatory responses in classically activated macrophages, lipopolysaccharides, and mycobacterial infection. *J. Immunol.* 194:6035–6044. http://dx.doi.org/10.4049/jimmunol.1402521

Sheikh, S.Z., K. Matsuoka, T. Kobayashi, F. Li, T. Rubinas, and S.E. Plevy. 2010. Cutting edge: IFN-γ is a negative regulator of IL-23 in murine macrophages and experimental colitis. *J. Immunol.* 184:4069–4073. http://dx.doi.org/10.4049/jimmunol.0903600

Stumhofer, J.S., A. Laurence, E.H. Wilson, E. Huang, C.M. Tato, L.M. Johnson, A.V. Villarino, Q. Huang, A. Yoshimura, D. Sehy, et al. 2006. Interleukin 27 negatively regulates the development of interleukin 17-producing T helper cells during chronic inflammation of the central nervous system. *Nat. Immunol.* 7:937–945. http://dx.doi.org/10.1038/ni1376

Su, Z.Z., S.G. Lee, L. Emdad, I.V. Lebdeva, P. Gupta, K.Valerie, D. Sarkar, and P.B. Fisher. 2008. Cloning and characterization of SARI (suppressor of AP-1, regulated by IFN). *Proc. Natl. Acad. Sci. USA.* 105:20906–20911. http://dx.doi.org/10.1073/pnas.0807975106

Tagawa, Y., K. Sekikawa, and Y. Iwakura. 1997. Suppression of concanavalin A-induced hepatitis in IFN-gamma(-/-) mice, but not in TNF-alpha(-/-) mice: Role for IFN-gamma in activating apoptosis of hepatocytes. *J. Immunol.* 159:1418–1428.

Tussiwand, R., W.L. Lee, T.L. Murphy, M. Mashayekhi, W. Kc, J.C. Albring, A.T. Satpathy, J.A. Rotondo, B.T. Edelson, N.M. Kretzer, et al. 2012. Compensatory dendritic cell development mediated by BATF-IRF interactions. *Nature.* 490:502–507. http://dx.doi.org/10.1038/nature11531

Villarino, A., L. Hibbert, L. Lieberman, E. Wilson, T. Mak, H. Yoshida, R.A. Kastelein, C. Saris, and C.A. Hunter. 2003. The IL-27R (WSX-1) is required to suppress T cell hyperactivity during infection. *Immunity.* 19:645–655. http://dx.doi.org/10.1016/S1074-7613(03)00300-5

Yoshimura, T., A. Takeda, S. Hamano, Y. Miyazaki, I. Kinjyo, T. Ishibashi, A. Yoshimura, and H. Yoshida. 2006. Two-sided roles of IL-27: Induction of Th1 differentiation on naive CD4+ T cells versus suppression of proinflammatory cytokine production including IL-23-induced IL-17 on activated CD4+ T cells partially through STAT3-dependent mechanism. *J. Immunol.* 177:5377–5385. http://dx.doi.org/10.4049/jimmunol.177.8.5377